Development 140, 2212-2223 (2013) doi:10.1242/dev.088260

Mechanisms of tentacle morphogenesis in the sea anemone *Nematostella vectensis*

Ashleigh E. Fritz[1,2], Aissam Ikmi[1], Christopher Seidel[1], Ariel Paulson[1] and Matthew C. Gibson[1,2,*]

SUMMARY

Evolution of the capacity to form secondary outgrowths from the principal embryonic axes was a crucial innovation that potentiated the diversification of animal body plans. Precisely how such outgrowths develop in early-branching metazoan species remains poorly understood. Here we demonstrate that three fundamental processes contribute to embryonic tentacle development in the cnidarian *Nematostella vectensis*. First, a pseudostratified ectodermal placode forms at the oral pole of developing larvae and is transcriptionally patterned into four tentacle buds. Subsequently, Notch signaling-dependent changes in apicobasal epithelial thickness drive elongation of these primordia. In parallel, oriented cell rearrangements revealed by clonal analysis correlate with shaping of the elongating tentacles. Taken together, our results define the mechanism of embryonic appendage development in an early-branching metazoan, and thereby provide a novel foundation for understanding the diversification of body plans during animal evolution.

KEY WORDS: *Nematostella vectensis*, Notch, Appendage evolution, Epithelial morphogenesis, Placode, Tentacle

INTRODUCTION

During development, changes in epithelial cell shape and cell number are central to the formation of organs and appendage structures. Studies of epithelial morphogenesis in bilaterian model systems have identified four basic mechanisms that initiate and drive organ and appendage outgrowth. First, changes in cell shape can dramatically alter the surface area of an epithelial sheet. For example, epithelial cells reduce the length of their apicobasal axis during wing morphogenesis in *Drosophila* and epiboly in *Xenopus*, resulting in increased surface area (Keller, 1980; Fristrom, 1988). Second, oriented cell division has been shown to direct tissue expansion during germband extension in *Drosophila* and primitive streak elongation in chick (Wei and Mikawa, 2000; da Silva and Vincent, 2007). Third, cell intercalation or convergent extension can longitudinally extend a tissue, such as during *Drosophila* embryonic germband extension and gastrulation in *Xenopus* (Keller, 1978; Irvine and Wieschaus, 1994). Fourth, many organ and appendage structures initiate morphogenesis as thickened epithelial placodes. In vertebrates, these include ectodermal appendages, such as teeth, feathers and scales, as well as the sensory placodes that give rise to structures such as the eye lens and inner ear (Baker and Bronner-Fraser, 2001; Pispa and Thesleff, 2003; Streit, 2007). Placodes are not only a vertebrate innovation; these structures also contribute to the development of *Drosophila* trachea and imaginal discs as well as sensory organs in ascidians (Fristrom, 1988; Manni et al., 2004; Franch-Marro et al., 2006). Nevertheless, most of our current knowledge about the molecular and cellular mechanisms involved in these morphogenetic processes has been elucidated in select bilaterian model systems.

To identify ancient pre-bilaterian mechanisms of epithelial morphogenesis, we are studying tentacle development in the cnidarian sea anemone *Nematostella vectensis* (Collins et al., 2006; Putnam et al., 2007; Dunn et al., 2008; Hejnol et al., 2009). Cnidarians are among the earliest branching metazoans with defined appendage structures used for prey capture and feeding. The adult *Nematostella* polyp exhibits 16 tentacles at the oral end of the animal, providing an ideal system with which to investigate mechanisms of epithelial morphogenesis during appendage development and regeneration. Furthermore, despite a deceptively simple diploblastic body plan, the *Nematostella* genome exhibits similar organization and content to that of vertebrates (Putnam et al., 2007). Accordingly, the genome encodes many proteins known to be involved in appendage development of arthropods and vertebrates, including a Hox gene cluster (Finnerty and Martindale, 1999; Chourrout et al., 2006), Fibroblast growth factors (FGFs) (Matus et al., 2007), Bone morphogenetic proteins (BMPs) (Rentzsch et al., 2006), Hedgehog (Hh) proteins (Matus et al., 2008), Wnts (Kusserow et al., 2005) and Notch pathway members (Marlow et al., 2012). At present, however, the contribution of these pathways to *Nematostella* tentacle development is largely unknown.

Cnidarians are broadly subdivided into two clades, Anthozoa (including sea anemones and corals) and the medusazoans (jellyfish and *Hydra* species) (Collins et al., 2006). Previous studies in hydrozoan systems have examined the origin of cells that populate and maintain tentacles. In these cases, tentacle growth was primarily studied in the context of adult homeostasis, regeneration and budding, but not as a result of embryonic development. In *Hydra*, interstitial stem cells (i-cells) and epithelial cells in the oral pole of the body column proliferate and move progressively up towards the tentacle zone (Campbell, 1967a; Campbell, 1967b; David and Challoner, 1974; David and Gierer, 1974; Bouillon, 1994). Once in the tentacle zone, they receive signals secreted from the hypostomal organizer (Broun and Bode, 2002), stop dividing, differentiate, and migrate into the tentacle (Campbell, 1967b; Holstein et al., 1991). A similar mechanism is observed in the jellyfish *Clytia*. In this case, populations of cells proliferate in a bulb at the base of the tentacle and then differentiate and move further into the tentacle itself (Denker et al., 2008). Although the degree of homology of polyp and medusa tentacles is still unclear, these two examples suggest

[1]Stowers Institute for Medical Research, 1000 E 50th Street, Kansas City, MO 64110, USA. [2]Department of Anatomy and Cell Biology, University of Kansas Medical Center, 3901 Rainbow Boulevard, Kansas City, KS 66160, USA.

*Author for correspondence (mg2@stowers.org)

Accepted 11 March 2013

a common mechanism in hydrozoans wherein tentacle growth and maintenance are driven by migration of progenitor cells that only proliferate outside of the tentacle.

Here, we show that the mechanism of *Nematostella* tentacle development does not involve localized cell proliferation as in Hydrozoa, but rather formation of a thickened ectodermal placode followed by changes in epithelial cell shape and cell arrangement along the oral-aboral axis. In a broader context, our findings hint at the ubiquity of fundamental aspects of epithelial morphogenesis throughout animals, and also define the formation of thickened epithelial placodes as a common initiating mechanism underlying outgrowth from the main body axes during animal development.

MATERIALS AND METHODS

Nematostella culture and differential interference contrast (DIC) imaging

Animals were raised at 16°C in 12 parts per thousand (ppt) artificial seawater (Sea Salt; Instant Ocean). Adult populations were spawned using an established protocol (Hand and Unlinger, 1992; Fritzenwanker and Technau, 2002). For imaging, planula larvae through four-tentacle primary polyps were relaxed in 7% $MgCl_2$ (Sigma) in artificial seawater for 10 minutes and fixed in 4% paraformaldehyde (Electron Microscopy Sciences) in artificial seawater for 1 hour at room temperature. Fixed specimens were washed three times in PTw (PBS with 0.1% Tween 20; Sigma), incubated in 87% glycerol (Sigma), mounted on glass slides and imaged on a Leica SP5 confocal microscope.

EdU incorporation in planula and primary polyps

Animals in artificial seawater were incubated with EdU (300 μM from a stock dissolved in DMSO) for 15 minutes (Click-it Alexa Fluor 488 Kit; Molecular Probes) as previously reported (Meyer et al., 2011). After incorporation, animals were relaxed in 7% $MgCl_2$ in artificial seawater for 10 minutes, fixed in cold 4% paraformaldehyde and 0.2% glutaraldehyde (Electron Microscopy Sciences) in artificial seawater for 90 seconds, and then 4% paraformaldehyde for 1 hour at room temperature. Specimens were washed three times in PBS and permeabilized in PBT (PBS with 0.5% Triton X-100; Sigma) for 20 minutes. The reaction cocktail was prepared based on the Click-it Kit protocol and incubated with the animals for 30 minutes. After three washes in PBS, the samples were labeled with Hoechst 34580 (1 μg/ml; Molecular Probes) in PBT overnight at 4°C. Animals were imaged on a Leica SP5 confocal microscope and *z*-stacks were made using Leica Application Suite Advanced Fluorescence (LAS AF) software.

Immunohistochemistry, RNA *in situ* hybridization and imaging

Animals were fixed and stained according to a protocol adapted from Genikhovich and Technau (Genikhovich and Technau, 2009a). After fixation, animals were stained with primary (mouse anti-α-Tubulin, 1:1000; Sigma) and secondary (goat anti-mouse IgG Alexa Fluor 488, 1:500; Molecular Probes) antibodies. Alexa Fluor 546 phalloidin (2 units/ml; Molecular Probes) was used to label F-Actin. Nuclei were counterstained with Hoechst 34580 (1 μg/ml; Molecular Probes). Animals were imaged on a Leica SP5 confocal microscope with LAS AF software.

For DAPI staining to mark cnidocytes, animals were fixed in 4% paraformaldehyde with 10 mM EDTA for 1 hour (Szczepanek et al., 2002; Marlow et al., 2009). They were washed four times in PBS and stored at 4°C. Before staining, animals were washed three times in PBT (PBS with 0.2% Triton X-100 and 0.1% BSA) and then incubated with DAPI (28 μM; Invitrogen) in PBT overnight at 4°C. After staining, animals were washed at least seven times in PBT. Animals were imaged as described above. DAPI was excited with both the UV and 488 confocal lasers.

RNA *in situ* probes were designed to cover at least 500 nucleotides. Regions were amplified from cDNA translated from total RNA (isolated from mixed stages of animals using the RNeasy Mini Kit; Qiagen) using the standard protocol of the OneStep RT-PCR Kit (Qiagen) and the primers listed in supplementary material Tables S2 and S3. Gene fragments were cloned into the TOPO-PCR4 sequencing vector (Invitrogen). Antisense probe was synthesized by *in vitro* transcription (MEGAScript Kit; Ambion) driven by T3 or T7 RNA polymerase with DIG incorporation (Roche). Probes were ethanol precipitated and resuspended in hybridization buffer to 50 ng/μl. RNA *in situ* hybridization was carried out as described (Genikhovich and Technau, 2009b). Briefly, animals were fixed in 0.2% glutaraldehyde and 3.7% formaldehyde (Sigma) in artificial seawater for 90 seconds and then in 3.7% formaldehyde in artificial seawater for 1 hour at room temperature. They were then washed, dehydrated in methanol (Sigma), and stored in methanol at −20°C until needed. Probes were hybridized to the animals for between 16 and 48 hours at 65°C. Animals were imaged on an Axiovert 200 widefield microscope with an Axiocam HRc camera using AxioVision software (Zeiss).

Microinjection

Unfertilized eggs were first dejellied in 4% cysteine solution (in artificial seawater, pH 7.4-7.6) for 10 minutes and then washed three times in artificial seawater (Fritzenwanker and Technau, 2002). Following dejellying, eggs were fertilized and injected with linearized ubiquitin-GFP plasmid (Mark Martindale, Kewalo Marine Laboratory, Honolulu, HI, USA) at 30 ng/μl using Femtojet Express (Eppendorf). Injected eggs were raised at room temperature in the dark and fixed at specific developmental stages for phalloidin staining: embryos, 24 hours; early planula larvae, 2 days; late planula larvae, 4 days; and primary polyps, 7-8 days.

Drug treatment of planula larvae

Prior to Cytochalasin D (Cyto D; Calbiochem) treatment, animals were raised for 10 days at 16°C in artificial seawater. Cyto D (1 μM) was applied in 0.1% DMSO in artificial seawater for 48 hours at room temperature in the dark. Concurrently, control animals were incubated in 0.1% DMSO in artificial seawater. Animals were fixed, stained and imaged as described above.

Prior to DAPT (Sigma) treatment, animals were raised for 8 days after spawning at 16°C in artificial seawater. They were incubated in 20 μM DAPT with 0.1% DMSO in artificial seawater for 2 days at room temperature in the dark. In parallel, control animals were incubated with 0.1% DMSO in 12 ppt artificial seawater.

Phenotypes following Cyto D or DAPT treatment were quantified by the percentage of animals that developed tentacles. To quantify the thickness of the body column ectoderm, animals from three independent experiments were measured using LAS AF software. Statistical analyses were performed using a Student's *t*-test.

Microarray design and data analysis

Total RNA was extracted from dissected animals using the miRNeasy Kit (Qiagen) with Trizol (Invitrogen). RNA quality was verified using a Bioanalyzer 2100 with Pico Total RNA chips (Agilent). RNA was amplified and labeled with Cyanine 3-CTP or Cyanine 5-CTP (Quick AMP Labeling Kit; Agilent). The array was designed in October of 2008 and comprised a 43,803 60-mer probe set targeting 43,787 sequences consisting of 20,456 JGI predictions and EST clusters, 16,816 StellaBase predictions, and 6515 UniGene predictions, EST clusters and mRNAs. This probe set was submitted to Agilent for their 4x44k platform under design ID: 022085. Microarray data were analyzed in the R environment. The linear modeling package Limma (Smyth, 2004) was used to derive gene expression coefficients and calculate *P*-values, which were adjusted for multiple hypothesis testing using the method of Benjamini and Hochberg (Benjamini and Hochberg, 1995). Genes were considered differentially expressed if they had adjusted *P*-values of less than 0.05 and an expression ratio of at least 2-fold in a given comparison. The data have been deposited in GEO with accession numbers: GSE45588 and GPL16896.

RESULTS

Cell proliferation is not spatially patterned in developing tentacles

Tentacle development in anthozoans has not been described in detail, and we therefore outlined the basic stages of this process in *Nematostella*. In early planula larvae, the first visible step in tentacle development was transition of the oral ectoderm to a

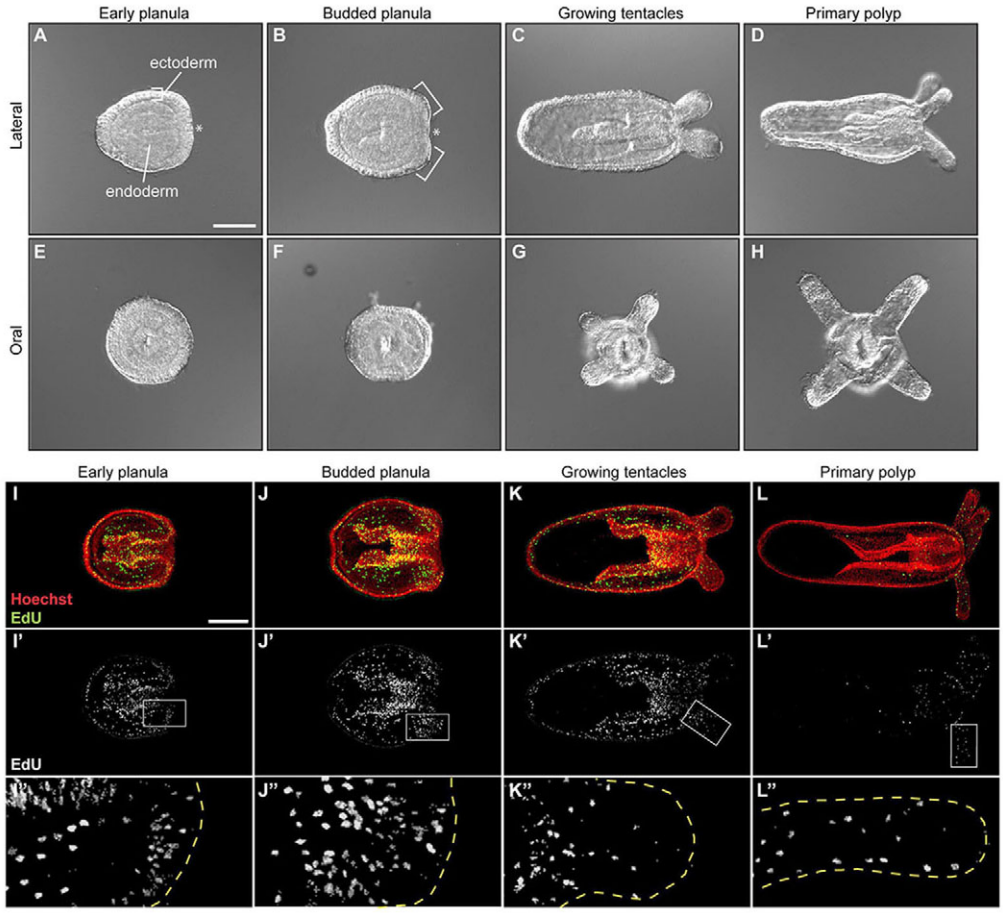

Fig. 1. Spatially uniform proliferation during tentacle development in *Nematostella*. (**A-H**) DIC images of lateral (A-D) and oral (E-H) views of animals during tentacle development at sequential stages: early planula (A,E), budded planula (B,F), growing tentacles (C,G) and primary polyp (D,H). *Nematostella* has two cells layers: the ectoderm and endoderm (A). Buds arise within the oral placodal ectoderm (brackets in B). These buds elongate from the body (C,D,G,H) to form the four primary polyp tentacles (D,H). The oral pole is indicated by asterisks and is oriented to the right in all lateral images. (**I-L**) Confocal *z*-stacks of animals stained for EdU incorporation (green) and with Hoechst to visualize S-phase cells and nuclei (red) at the indicated sequential stages during tentacle development. (**I′-L′**) The EdU channel from I-L shows that there are no spatially restricted populations of proliferating cells. (**I″-L″**) Magnification of the boxed regions from I′-L′. EdU-positive cells can be seen in the growing and mature tentacles (see K″ and L″). The outline of the animal is indicated (dashed line). Scale bars: 100 μm.

thickened, epithelial placode (Fig. 1A,E). In slightly later stages, the first four tentacle buds arose from within this region (Fig. 1B,F, brackets), and subsequently grew out from the body (Fig. 1C,G) and elongated into the four juvenile tentacles (Fig. 1D,H). At this stage, planula larvae settled and further growth and differentiation took place to form the four-tentacle juvenile polyp. Concurrent with tentacle elongation, we noted that the body column also progressively elongated along the oral-aboral axis (Fig. 1C,D). Additionally, the endoderm thinned along with the ectoderm, although this cell layer was not as rigidly organized (supplementary material Fig. S1). Importantly, all developmental events to this point took place in the absence of feeding, whereas the subsequent addition of tentacles and their growth were nutrient dependent (data not shown).

A general theme emerges from previous analyses of tentacle maintenance in adult hydrozoan cnidarians, wherein specific populations of proliferating progenitor cells stop dividing, differentiate, and migrate into the tentacles (Campbell, 1967a; Campbell, 1967b; Holstein et al., 1991; Denker et al., 2008). However, given the substantial evolutionary distance between Hydrozoa and the more basal Anthozoa (Collins et al., 2006; Putnam et al., 2007), highly divergent mechanisms could govern tentacle morphogenesis in each group. To determine whether *Nematostella* tentacle outgrowth or maintenance involves a similar mechanism of progenitor cell proliferation and migration, we isolated animals from the early planula through primary polyp stages and visualized S-phase incorporation of the nucleotide analog EdU. Throughout tentacle development, cell proliferation occurred in both the ectoderm and endoderm all along the body column (Fig. 1I-L′). Unlike the previously studied hydrozoan systems, cell proliferation was not obviously localized to any specific region in the developing animal. Additionally, we observed EdU-positive cells in the tentacle ectoderm at all stages analyzed, consistent with continuous heterogeneous proliferation throughout development (Fig. 1I″-L″).

Radical changes in the apicobasal thickness of ectodermal cells during tentacle elongation

Although we did not identify localized domains of cell proliferation correlating with tentacle outgrowth, we did observe striking changes in the morphology of ectodermal epithelial cells during this process. To investigate this further, we tracked cytoskeletal dynamics using

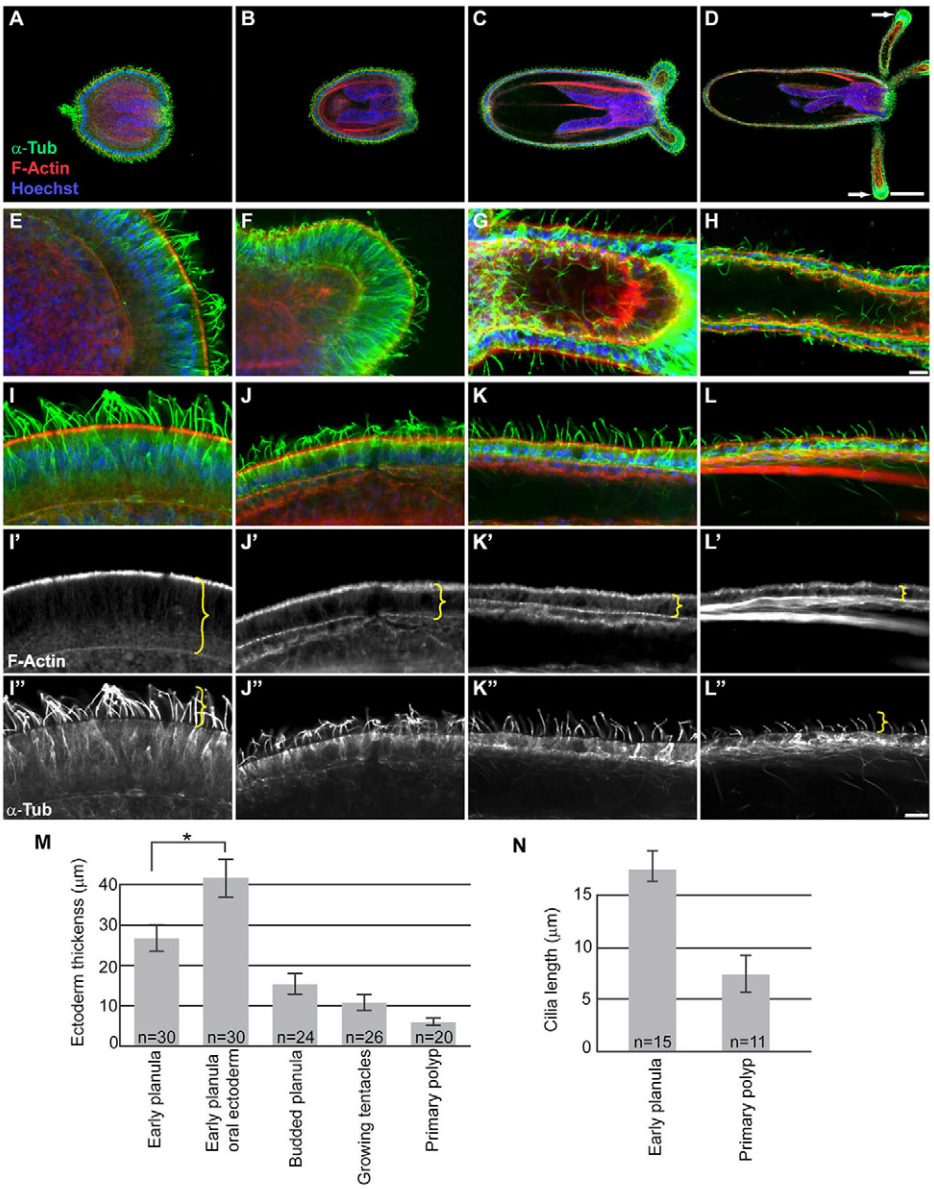

Fig. 2. Changes in ectodermal morphology during tentacle and body column elongation. (**A-D**) Confocal sections of whole animals stained with an antibody against α-Tubulin (α-Tub; green), phalloidin to visualize F-Actin (red), and Hoechst to label nuclei (blue) at sequential stages: early planula (A), budded planula (B), growing tentacles (C) and primary polyp (D). Arrows (D) indicate lack of flattening of cells in the tentacle tips. (**E-H**) Confocal sections of buds or tentacles at stages corresponding to A-D. Cells in the ectoderm change apicobasal dimension during tentacle development. (**I-L**) Similar cell shape changes are seen in the body column ectoderm at corresponding stages. (**I′-L′**) The F-Actin channel of I-L demonstrating the thickness of the ectoderm (brackets). (**I″-L″**) Ectodermal cell cilia, as visualized by α-Tubulin staining, shorten during body column elongation. Brackets indicate length of cilia. (**M**) Quantification of body column and oral ectodermal thickness during elongation at stages corresponding to A-D. *P<0.001 (Student's t-test). (**N**) Quantification of cilia length from early planula and primary polyp stages. Error bars represent s.d.; n, number of individuals examined for each stage. Scale bars: 100 μm in D; 10 μm in H,L″.

probes for both Actin and Tubulin. At the early planula stage, before the initiation of tentacle development, cells in the body column and oral ectoderm constituted a thickened, pseudostratified epithelium (Fig. 2A,E,I) (Meyer et al., 2011). Just prior to tentacle bud formation, the oral ectoderm thickened in comparison to the body column, and the first four tentacle buds formed within this oral epithelial placode (Fig. 2B,F, quantified in 2M). As the buds elongated into tentacles, we observed a concomitant progression of the thickened, pseudostratified ectoderm into a simple columnar, then cuboidal and finally a more flattened morphology (Fig. 2F-H). Interestingly, cells in the tentacle tips did not flatten (Fig. 2D, arrows), perhaps allowing for a higher density of nematocysts used for prey capture. Similar cellular events were observed in the body column ectoderm during elongation of the oral-aboral axis (Fig. 2I-L). Early in larval development the thickness of the body column ectoderm averaged 27.2±3.2 μm, which thinned to an average of only 6.2±0.9 μm by the primary polyp stage (Fig. 2I′-L′, quantified in 2M). Interestingly, during the progressive thinning of the ectodermal epithelium, the cilia associated with these cells also became progressively shorter (Fig. 2I″-L″, quantified in 2N).

Actin dynamics are required for elongation of the body column and tentacles

The observations above suggest that changes in ectodermal cell shape could vastly increase the surface area of primary polyps, thereby representing a primary driver of tentacle outgrowth and elongation of the body column. To functionally test the role of cell shape changes during elongation, we disrupted Actin polymerization with Cytochalasin D (Cyto D; 1 mM in 0.1% DMSO) (Casella et al., 1981). For these experiments, animals were raised at 16°C for 10 days post-fertilization, and then swimming planula were treated with Cyto D for 48 hours during the period of normal cell shape change and elongation (Fig. 3A). Control animals elongated their body columns and formed growing tentacles in these 2 days (Fig. 3B), but animals treated with Cyto D were unable to form tentacles or elongate the body column (Fig. 3C, quantified in 3E). These defects correlated with a block in epithelial morphogenesis. Whereas the ectoderm of control animals thinned normally (Fig. 3A′,B′), drug-treated animals retained a thickened, pseudostratified epithelium (Fig. 3C′, quantified in 3F).

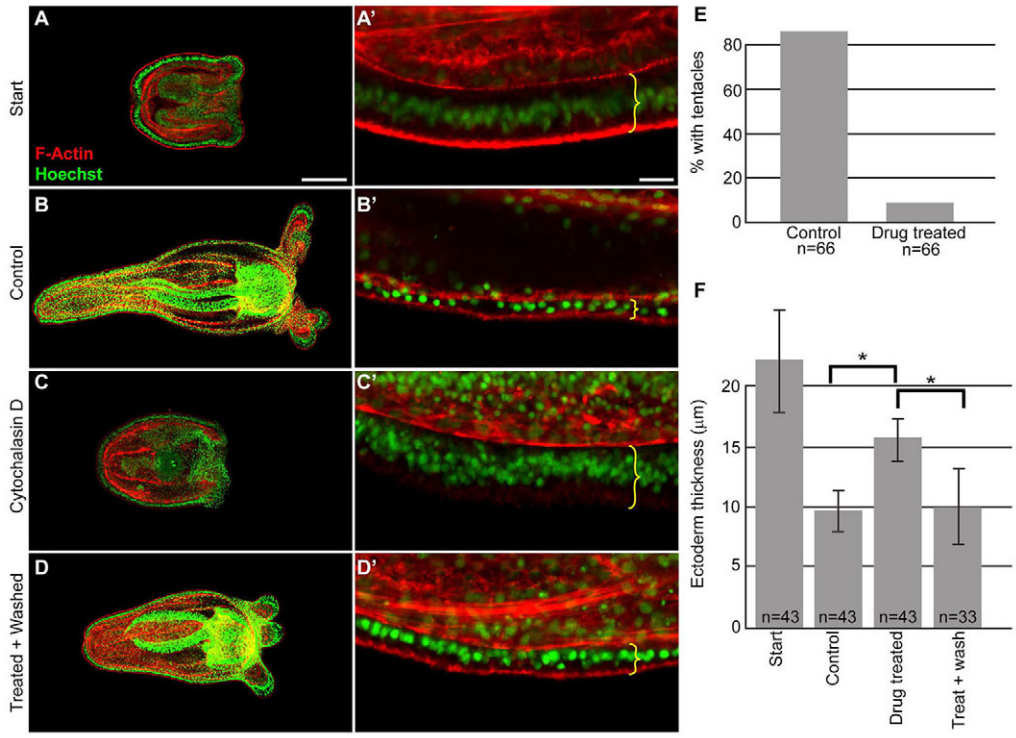

Fig. 3. Cytochalasin D treatment of planula larvae inhibits ectodermal cell shape changes. (**A-D**) Confocal sections of whole-mount animals stained with phalloidin to label F-Actin (red) and Hoechst to visualize nuclei (green). (**A′-D′**) Magnified view of body column ectoderm from animals corresponding to A-D. Brackets indicate ectodermal thickness. Animals were treated at the planula stage (A,A′). Control animals elongated their body columns and grew tentacles (B,B′). Cytochalasin D (Cyto D)-treated animals were unable to elongate their body columns or grow tentacles (C,C′). This was accompanied by a lack of cell shape change in the ectoderm (compare C′ with the control in B′). Animals recovered after Cyto D was washed off (D,D′). (**E**) Phenotype of the Cyto D-treated animals was quantified by the percentage of animals that developed tentacles. (**F**) Apicobasal thickness of the body column ectoderm in Cyto D-treated animals. *P<0.001 (Student's t-test). The ectoderm of control, Cyto D-treated, and Cyto D-treated + wash animals was significantly thinner than at the start point. The Cyto D-treated animals had a significantly thicker body column ectoderm than controls. The treated + wash animals were able to thin the ectoderm to a thickness similar to that of controls. Error bars represent s.d.; n, number of individuals examined for each condition. Scale bars: 100 µm in A; 10 µm in A′.

Additionally, we examined cell proliferation by EdU incorporation in the Cyto D-treated and control animals. Although there was still some cell proliferation after Cyto D treatment, it was reduced compared with that in control animals (supplementary material Fig. S2). Intriguingly, upon removal of the drug treatment, these animals were able to continue development to become primary polyps (Fig. 3D). These changes directly correlated with a thinning of the ectoderm into a more flattened epithelium as in controls (Fig. 3D′, quantified in 3F).

Combined, these results indicate that Actin polymerization is required for changes in ectodermal cell shape and the associated elongation of the body column and tentacles.

Elongation is directed by cell rearrangements and orientated cell division

Although a dramatic reduction in apicobasal thickness of ectodermal cells can account for an increase in surface area of the entire animal, it cannot explain the directional expansion along the oral-aboral axis. To address how this is achieved, we used mosaic expression analysis. We microinjected one-cell stage embryos with a construct expressing Green fluorescent protein (GFP) under the control of the *Nematostella ubiquitin* promoter, taking advantage of the resulting mosaic expression of GFP to observe the behavior of cell clones. Strikingly, there were clear changes in the shape of GFP-expressing clones at different stages of body column and tentacle elongation (Fig. 4; supplementary material Fig. S3). At both embryonic and early planula larvae stages, animals had irregular but largely isometrically shaped GFP-expressing clones (Fig. 4A-B′; supplementary material Fig. S3A,B). As late planulae began to undergo elongation of the body column and tentacles, we observed both irregularly shaped and elongated clones (Fig. 4C,C′; supplementary material Fig. S3C). Intriguingly, by the primary polyp stage almost all clones comprised linear arrays of cells stretching along the oral-aboral axis in both the body column and tentacles (Fig. 4D,D′; supplementary material Fig. S3D).

The rearrangement of cell clones into linear oral-aboral morphologies could be explained by cell rearrangements, such as convergent extension, or by oriented cell division. To distinguish between these two possibilities, we analyzed the orientation of cell division during elongation of the body column and tentacles. In order to determine the angle of the spindle, animals from embryonic to primary polyp stages were stained to visualize microtubules and DNA, thus revealing the orientation of metaphase and anaphase figures. The angle of the spindle was measured in degrees from the oral-aboral axis for the body column (supplementary material Fig. S4A,A′). Whereas the spindle orientation early in development was random (Fig. 5A-B), spindle orientations became biased along the oral-aboral axis during body

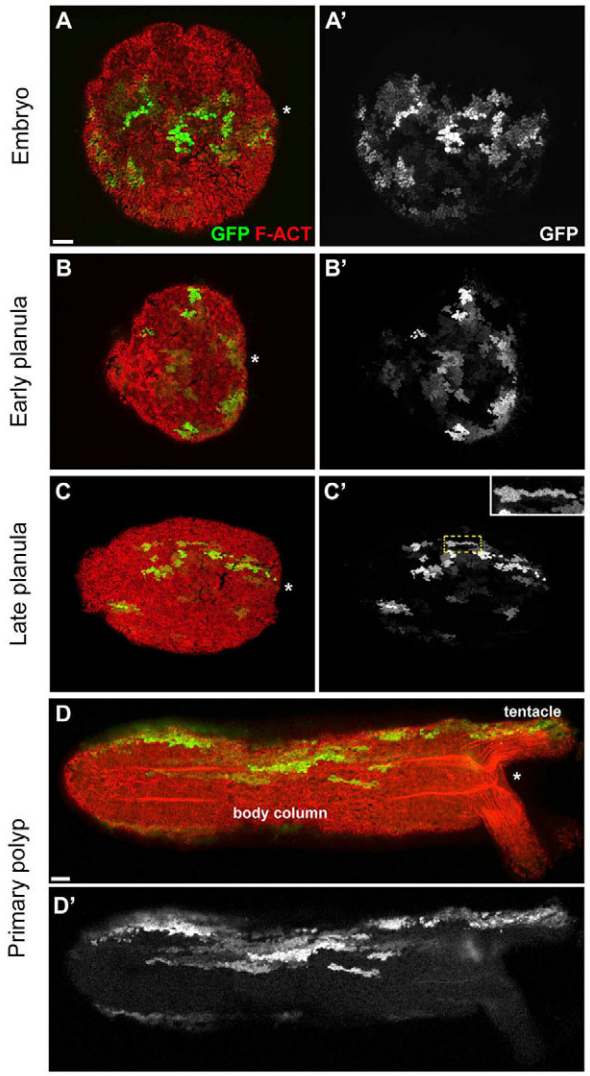

Fig. 4. Analysis of ectodermal cell clones during body column and tentacle elongation. GFP-marked cell clones (green) in representative animals stained with phalloidin to label F-Actin (red). Ectodermal surface views are shown. (**A**,**A′**) Embryos exhibited irregular and largely isometric clone morphologies. (**B**,**B′**) In early planula, the clone shape was not significantly different from that of the embryo. (**C**,**C′**) By the late planula stage, cell clones appeared to elongate along the oral-aboral axis. The inset shows a clone of GFP-positive cells with both a rounded shape and a linear array of cells extending along the oral-aboral axis. (**D**,**D′**) Primary polyps had highly elongated clone shapes. Asterisks indicate the position of the oral pole. Scale bars: 25 μm.

column elongation (Fig. 5C-F). As elongation progressed in the budded planula stage, this bias weakened and spindle orientation became more random (Fig. 5G-I). Additionally, we measured the angles of mitotic spindles in the tentacle buds and tentacles in degrees from the proximodistal axis (see supplementary material Fig. S4B,C). Interestingly, here we did not observe any bias in spindle orientation (Fig. 5J-M).

Taken together, these results suggest that both cellular rearrangements and oriented cell division play a role in elongation of the body column. In developing tentacles, however, we found evidence for cellular rearrangements but did not observe a bias in mitotic spindle orientation.

Notch signaling is required for tentacle elongation

A relatively limited set of developmental signaling pathways regulates the patterning and morphogenesis of tissues and organs in all animals (Gerhart, 1999; Pires-daSilva and Sommer, 2003). Interestingly, the transmembrane receptor Notch and its ligand Delta are expressed orally and around the tentacle primordia in *Nematostella* larvae (Marlow et al., 2012). To investigate the role of Notch during tentacle morphogenesis, we modulated signaling using a pharmacological inhibitor, DAPT (Dovey et al., 2001; Käsbauer et al., 2007; Marlow et al., 2012). DAPT inhibits γ-secretase, the enzyme responsible for cleaving the Notch intracellular domain (NICD) (Geling et al., 2002). We applied 20 μM DAPT in 0.1% DMSO to planula stage animals for 2 days during the expected period of body column and tentacle elongation (Fig. 6A). As expected, control animals elongated their body columns and formed growing tentacles in these 2 days (Fig. 6B,B′), morphogenetic events that were accompanied by changes in ectodermal cell shape (Fig. 6B″). By contrast, DAPT-treated animals failed to develop tentacles (Fig. 6C, quantified in 6D) and the oral ectoderm retained its thickened tentacle buds (Fig. 6C′). Surprisingly, although normal morphogenesis of the tentacle ectoderm was blocked, DAPT-treated animals exhibited normal thinning of the body column ectoderm and were still able to elongate their body columns along the oral-aboral axis (Fig. 6C,C″, quantified in 6E). Additionally, cell proliferation and cnidocyte localization appeared unaffected (supplementary material Figs S5, S6). These unexpected results demonstrate that epithelial shape changes in the body column and tentacular ectoderm are subject to distinct forms of upstream regulation. Specifically, disruption of Notch signaling did not affect the cell shape changes or elongation of the main body column, but did have a dramatic effect on cell shape change and elongation of the tentacles. These results further support the hypothesis that the cell shape change in the ectoderm is important for elongation because the tentacle buds remained thickened and did not elongate from the body (Fig. 6B′,C′).

Notch signaling generally acts through activation of downstream transcriptional targets, and we therefore sought to identify factors modulated by DAPT treatment. We examined the expression patterns of six previously identified tentacle domain markers and confirmed that the homeodomain transcription factor *OtxB* is expressed in developing tentacle buds and at the tips of tentacles in primary polyps (Mazza et al., 2007) (Fig. 6F,G; supplementary material Table S1). In animals treated with DAPT for 48 hours at the planula stage, *OtxB* was no longer expressed in the tentacle buds. Instead, we observed *OtxB* misexpression in the oral pole of the mesenteries, which are internal endomesodermal structures (Fig. 6H). These results imply a role for Notch signaling in regulating the expression of *OtxB*. None of the other genes that we examined had detectable changes in their expression domain with DAPT treatment (supplementary material Table S1), suggesting that tentacle patterning was not completely disrupted by inhibition of Notch.

Additionally, we examined the expression patterns of Notch pathway components after DAPT treatment. *Notch*, *Delta* and *HES3* did not appear to have qualitatively altered expression patterns (supplementary material Fig. S7). However, as expected, *HES3* levels were reduced after DAPT treatment (see supplementary material Fig. S7C,F), and our results suggest that *Notch* and *Delta* are also downregulated after inhibiting the pathway (supplementary material Fig. S7A,B,D,E).

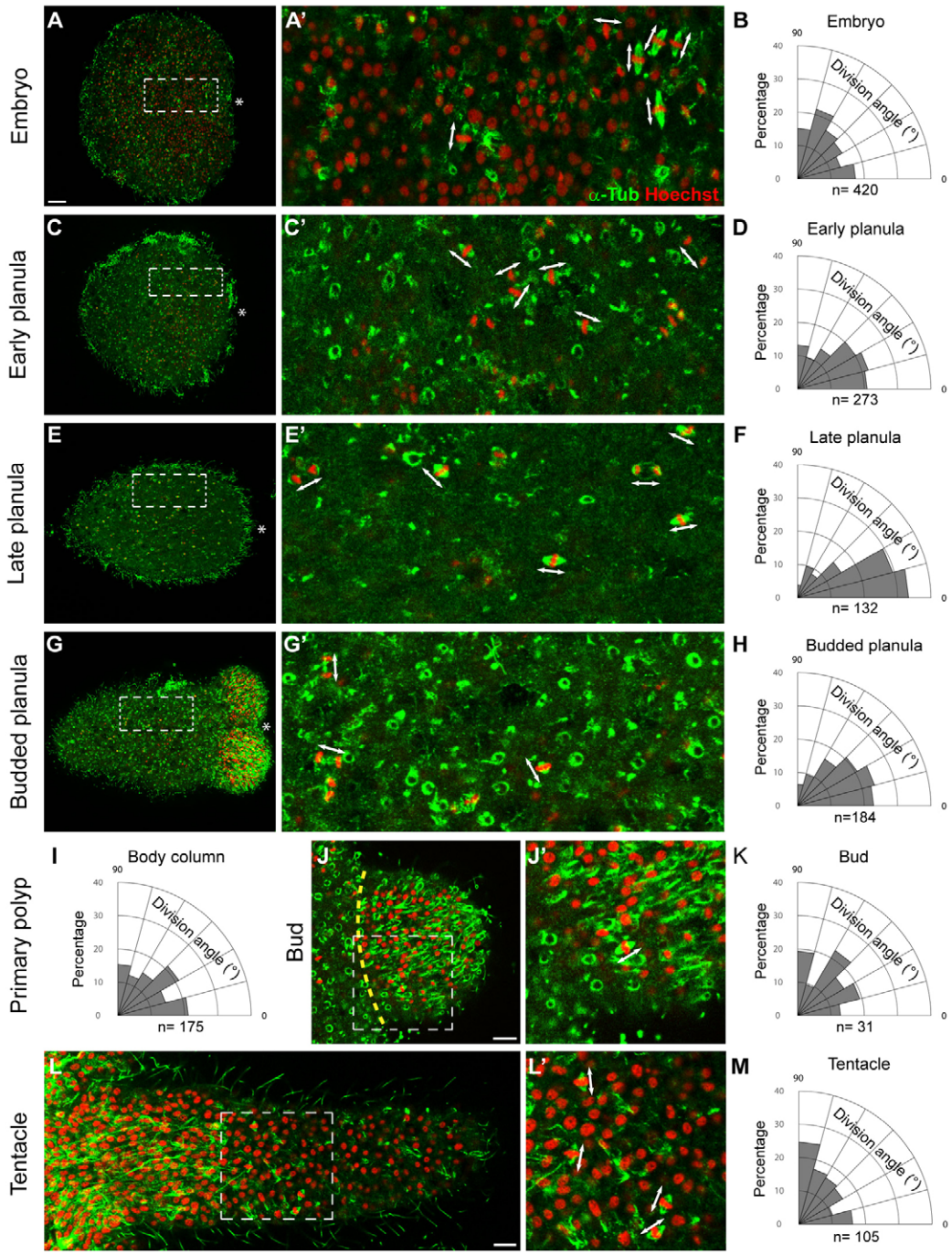

Fig. 5. Orientation of ectodermal cell division during *Nematostella* development. (**A-I**) Animals were stained for α-Tubulin to label mitotic spindles (green) and Hoechst to label nuclei (red). Orientation of the mitotic spindles was measured in embryos (A-B), early planula larvae (C-D), late planula larvae (E-F), budded planula larvae (G-H) and primary polyps (I). Asterisks indicate the oral pole. The boxed regions in A,C,E,G are magnified in A′,C′,E′,G′ to show detailed views of the ectoderm. Double-headed arrows indicate mitotic figures as well as the orientation of the mitotic spindle. The angular deviation of the mitotic spindle was measured as degrees from the oral-aboral axis (B,D,F,H,I). *n*, number of mitotic figures used for quantification. Note the strong alignment of mitotic spindles along the oral-aboral axis in late planula stage animals (E-F). (**J-M**) Angular deviation of mitotic spindle alignment from the proximodistal axis of tentacle buds (J-K) and mature tentacles (L-M). The boxed regions in J and L are magnified in J′ and L′. The dashed line in J indicates the approximate boundary of the bud. The small green α-Tubulin-positive rings are nematocyst capsules. Scale bars: 25 μm.

Unbiased identification of tentacle-specific genes by transcriptional profiling

To gain further insight into the transcriptional programs underlying tentacle morphogenesis and Notch signaling, we identified novel tentacle markers that could be used to screen following DAPT treatment. To take an unbiased approach, we designed a novel microarray from the sequences deposited in three publically available databases: the Joint Genome Institute (JGI), National Center for Biotechnology Information (NCBI) and Stellabase (Sullivan et al., 2006; Sullivan et al., 2008). To identify genes potentially involved in tentacle initiation, outgrowth and maintenance, we performed transcriptional profiling at three different stages: late planula larvae with tentacle buds; animals with growing tentacles; and four-tentacle polyps (Fig. 7A). In each case, animals were microdissected with a tungsten needle to isolate tentacle tissue from the rest of the larval body. Each animal was bisected perpendicular to the main body axis at the base of the tentacles, generating cognate body column and oral-tentacle fragments (Fig. 7A). RNA was isolated from each sample and subjected to a single round of amplification, dye labeling and hybridization to a microarray chip in duplicate (supplementary material Fig. S8). We found that many of the genes in the oral body portion were common among the different stages of development, suggesting they are consistently expressed during tentacle initiation, elongation and maintenance (Fig. 7B).

For bioinformatics analysis of the results, highly differentially expressed sequences were manually subjected to a BlastX search at NCBI to look for similarity to any known proteins in the non-

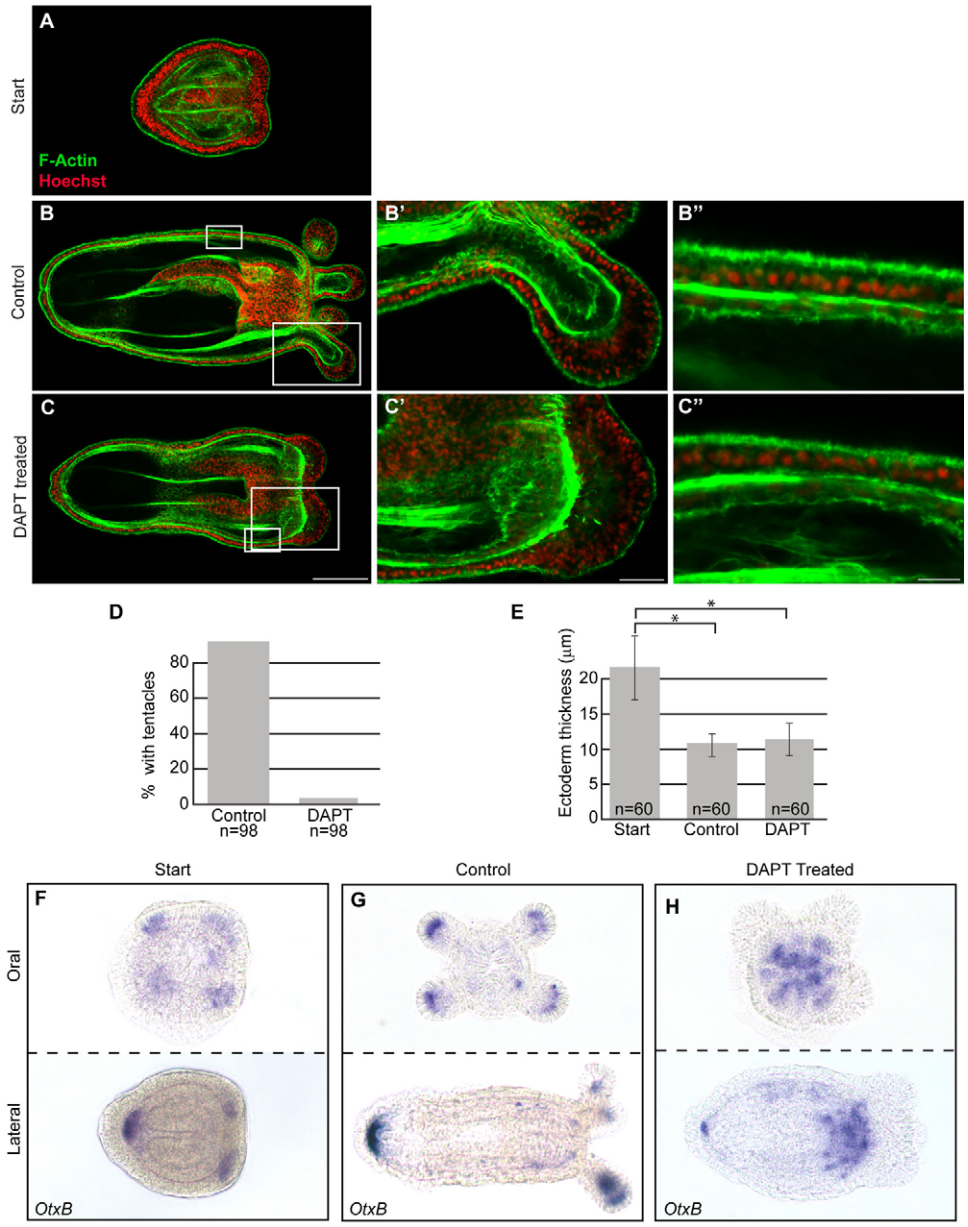

Fig. 6. Notch signaling is required for tentacle elongation. (**A-C**) Confocal sections of whole animals stained with phalloidin to visualize F-Actin (green) and Hoechst to label nuclei (red). (**B′**,**C′**) Higher magnification confocal sections of the tentacle regions indicated by the larger boxes in B and C. (**B″**,**C″**) Higher magnification confocal sections of the body column ectoderm indicated by the smaller boxes in B and C. Animals were treated at the planula stage (A). Control animals had growing tentacles (B,B′) and elongated body columns, which had undergone a cell shape change (B″). DAPT-treated animals remained budded and were unable to elongate tentacles (C,C′), but still elongated their body columns and underwent a cell shape change (C,C″). (**D**) The percentage of animals that developed tentacles in the presence and absence of DAPT. (**E**) Quantification of body column ectoderm thickness. Errors bars represent s.d.; *n*, number of individuals examined in each condition. **P*<0.001 (Student's *t*-test). The body column ectoderm thickness was similar in control and DAPT-treated animals and significantly thinner than at the start point. (**F-H**) Oral (top row) and lateral (bottom row) views of RNA *in situ* hybridization with probes for *OtxB*. *OtxB* is normally expressed in the tentacle primordia (F) (Mazza et al., 2007) and then at the tips of the tentacles (G). It was also expressed at the aboral pole throughout development (F,G). After DAPT treatment, *OtxB* was misexpressed in the oral regions of the mesenteries, but aboral expression was maintained (H). Scale bars: 100 µm in C; 25 µm in C′; 10 µm in C″.

redundant database. Additionally, the nucleotide sequence for each potential hit was blasted against the *Nematostella* EST database (NCBI) and EST clusters at JGI. Lastly, we used the protein sequence of candidate genes to identify conserved domains and to extract functional information using InterProScan from the European Bioinformatics Institute.

We chose 50 candidate genes to validate by RNA *in situ* hybridization. Attractive candidates included sequences with the highest fold change values or that contained transcription factor or signaling molecule domains. From these, we identified six genes not previously known to have tentacle domain expression patterns (Fig. 7C-H; supplementary material Table S2). Two of these were previously identified genes, but were not known to have tentacle-specific expression: *anthox2* (AF085283.1; Fig. 7C) (Finnerty et al., 2003; Ryan et al., 2006) and *foxL2* (JGI: 82873608; Fig. 7D) (Magie et al., 2005). Two of the six contained forkhead domains, which we called *forkhead1* (XM_001630267.1; Fig. 7E) and *forkhead2* (XM_001638841.1; Fig. 7F). Of the remaining two, one contained a growth factor receptor domain (*growth factor receptor-like*; XM_001637818; Fig. 7G) and the other contained a G protein receptor domain (*g protein receptor-like*; XM_001636348.1; Fig. 7H).

Most of these genes were expressed early in some or all of the oral placodal ectoderm before bud formation, and then exhibited bud-specific expression when the tentacle primordia formed (Fig. 7C-F,H). However, *growth factor receptor-like* was expressed ubiquitously in the endoderm until the growing tentacle stage, when it also became expressed in the tips of the tentacle endoderm (Fig. 7F). When we screened these genes for changes in expression pattern after DAPT treatment, none changed (supplementary material Table S1), suggesting that tentacle patterning was not disrupted following inhibition of Notch signaling.

From the expression patterns of these genes, as well as those previously published in the literature, we propose a model for tentacle patterning whereby the oral tissue is progressively subdivided into tentacle-competent and non-competent domains (Fig. 7I).

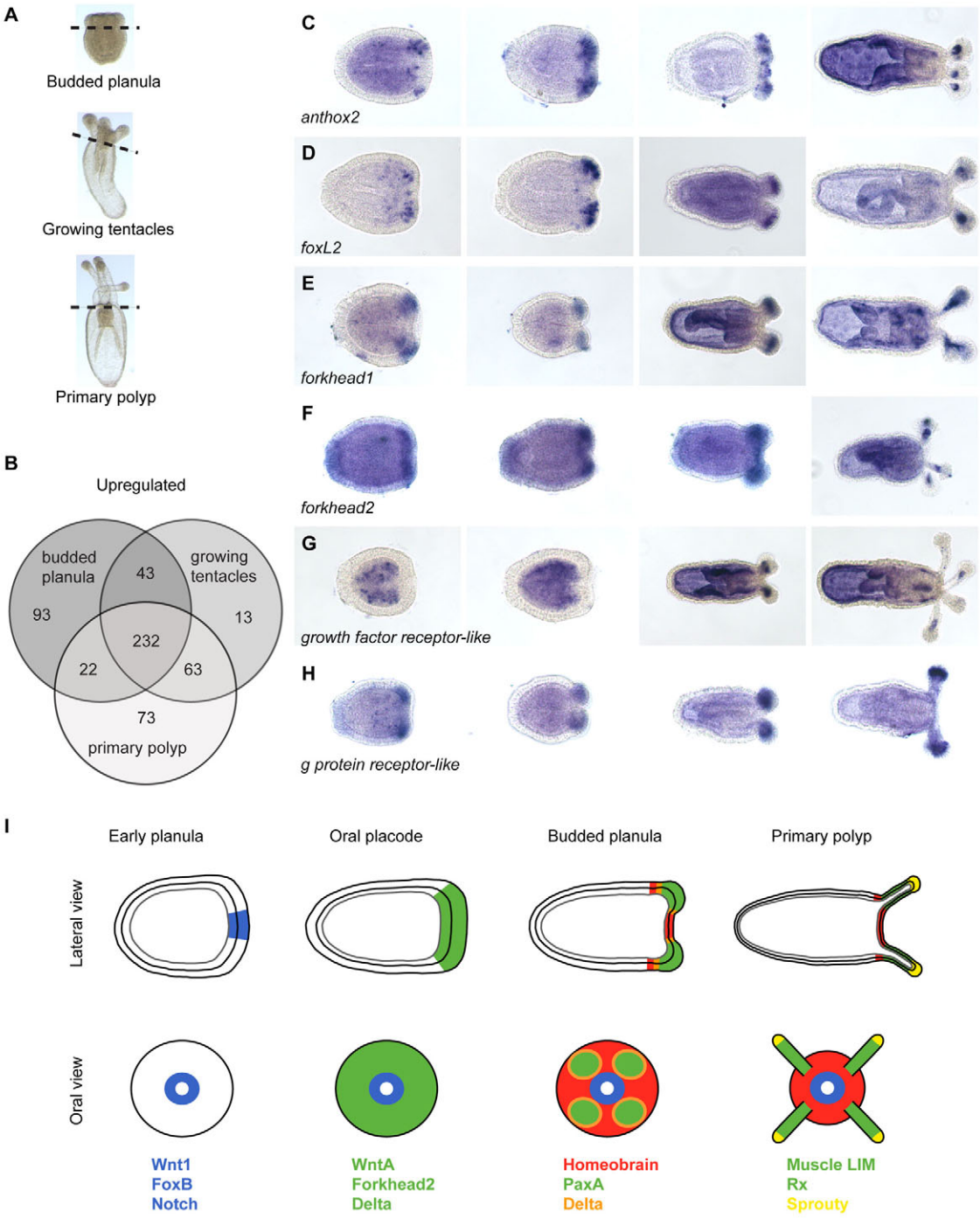

Fig. 7. An unbiased screen for novel tentacle markers. (**A**) The budded planula, growing tentacles and primary polyp stages were used to identify novel tentacle-specific genes by transcriptional profiling. Animals were dissected at the base of the tentacles (dashed line) and gene expression differences between the tentacle domain and corresponding body column were measured using custom microarrays in duplicate. (**B**) Venn diagram of the transcripts that were at least 2-fold upregulated in the oral/tentacle tissues from the three stages examined. A large proportion of the tentacle-specific genes was common to all stages, suggesting an absence of major transcriptional changes underlying successive stages of development. (**C-H**) From left to right: early planula, budded planula, growing tentacles and primary polyp stages. RNA *in situ* hybridization of tentacle marker genes identified from the microarray analysis. Most of these genes were expressed early in the oral placodal ectoderm before being expressed in the tentacle buds (C-F,H). *growth factor receptor-like* was expressed in the endoderm early, before exhibiting endodermal tentacle tip expression in primary polyps (G). (**I**) A conceptual model for tentacle patterning in which oral cells are subdivided into tentacle-competent and non-competent domains. In early planulae, genes such as *FoxB* (Magie et al., 2005), *Wnt1* (Kusserow et al., 2005) and *Notch* (Marlow et al., 2012) are expressed orally (blue). At the oral placode stage, genes such as *WntA* (Kusserow et al., 2005), *forkhead2* and *Delta* (Marlow et al., 2012) are expressed broadly in the oral placode (green). Once budded, planula larvae express a subset of genes in the buds, such as *PaxA* (Magie et al., 2005) (green), between the buds, such as *homeobrain* (Mazza et al., 2010) (red), and encircling the buds, such as *Delta* (Marlow et al., 2012) (orange). Patterning becomes more complicated at the primary polyp stage, when some genes are expressed along the length of the tentacle, such as *muscle LIM* and *Rx* (Martindale et al., 2004; Mazza et al., 2010) (green), or at the tips of the tentacles, such as *sprouty* (Matus et al., 2007) (yellow).

DISCUSSION

A new model for pre-bilaterian appendage development

Our results establish a novel model for tentacle morphogenesis in *Nematostella*. The initial step in tentacle development is the formation of a thickened ectodermal placode at the oral pole of the animal ~5 days after fertilization at 16°C (Fig. 1A; Fig. 2A,E). This placode is progressively subdivided into four distinct tentacle domains (Fig. 1B; Fig. 2B,F), presumably through the spatially restricted expression of key effector genes (Fig. 7C-I). Once the tentacle buds are formed, Notch signaling activity is required to trigger apicobasal thinning of the tentacular ectoderm (Fig. 6A-E), radically increasing the surface area of the presumptive tentacle. Actin dynamics are required for this process to occur in both the body column and oral ectoderm (Fig. 3), and cell proliferation occurs stochastically along the length of the tentacle throughout development (Fig. 1K-L). Cell lineage-tracing experiments further reveal a concomitant axial rearrangement of cell clones from irregular and isometric (Fig. 4A,B) to linear (Fig. 4C,D) morphologies during tentacle outgrowth. We propose that these changes in epithelial architecture of the oral ectoderm contribute to elongation of the tentacles. Intriguingly, although elongation of the main body column appears to involve oriented cell division (Fig. 5E-H), we did not observe oriented cell division in the tentacles (Fig. 5J-M).

Currently, we do not have sufficient molecular data from *Nematostella* appendage development or from other basal metazoans to make a comparison with bilaterian appendage development. Even though arthropod appendages and vertebrate limbs are not homologous, both exhibit *distalless*/*Dlx* expression at the presumptive distal portion of the appendage (Angelini and Kaufman, 2005; Kraus and Lufkin, 2006). The published RNA expression pattern of the *Nematostella Dlx* homolog does not show expression at the tentacle tips or in any tentacle tissue during development (Ryan et al., 2007). Our current data would not support a model in which *Nematostella* tentacles are homologous to any of the bilaterian appendages, but more data from *Nematostella* as well as other basal metazoan species are still needed.

Notch signaling and tentacle elongation

Pharmacological inhibitor studies with DAPT indicate a key role for Notch signaling in tentacle elongation (Fig. 6A-E). Consistent with this, Notch pathway components are expressed in the oral and tentacle bud ectoderm prior to and during metamorphosis (Marlow et al., 2012), and signaling through this pathway is generally known to affect downstream transcription (Petcherski and Kimble, 2000; Wu et al., 2000; Artavanis-Tsakonas and Muskavitch, 2010). When we inhibited Notch signaling, the tentacle bud expression of *OtxB* was disrupted (Fig. 6F-H). Additionally, Notch signaling restricts *PaxA* expression to the tentacle primordia (Marlow et al., 2012). These results indicate that Notch signaling directly or indirectly leads to the specific tentacle expression patterns of these genes.

However, our results do not support the hypothesis that Notch signaling is required for global tentacle patterning, as many other tentacle markers were unaffected by Notch inhibition (supplementary material Table S1). A previous study of Notch signaling in *Nematostella* reported fused tentacles and an expanded tentacle field (based on *PaxA* expression) following 72 hours of DAPT treatment (10 μM in 1% DMSO) in 3-day post-fertilization planulae raised at 25°C. By contrast, we used 8-day-old planula larvae raised at 16°C, and treated them with a tenth of the concentration of DMSO but a higher concentration of DAPT for 48 hours. Given these differences, our data do not support a general expansion of the tentacle field following DAPT treatment, as numerous tentacle markers did not change in expression pattern and our animals developed four tentacle buds that failed to elongate (Fig. 6).

Nematostella and *Hydra* tentacle development are likely to occur through different mechanisms

In hydrozoans, tentacle development has mainly been studied in adult animals, in regeneration and in the asexual budding of polyps, but not during embryonic development. *Hydra* polyps continuously replace all of the cells in their bodies with cells derived from their i-cells and from constantly dividing epithelial cells (David and Campbell, 1972; David and Murphy, 1977; Bode and David, 1978). This is unlikely to be the case in *Nematostella*, in which i-cells have not been identified. Another hallmark of *Hydra* tentacle development and maintenance is a distinct border at the tentacle zone. This is delineated by an absence of cell division and sharply defined gene expression domains (Holstein et al., 1991; Smith et al., 1999; Bode, 2001). Based on our EdU staining results as well as known expression patterns, we find no evidence for a 'tentacle zone' in *Nematostella* during development or adult maintenance. Furthermore, in *Hydra*, activation of canonical Wnt signaling is sufficient to cause tentacle outgrowth along the body column (Hassel et al., 1993; Broun et al., 2005). By contrast, recent studies in *Nematostella* show that ectopic activation of canonical Wnt signaling can only induce tentacle and oral fates at the aboral pole of developing animals, not along the body column (Trevino et al., 2011). Additionally, we have demonstrated that Notch signaling is required for tentacle elongation in *Nematostella* (Fig. 6A-E). Notch signaling in *Hydra* is important for stem cell development and detachment of the asexual bud from the parent animal (Käsbauer et al., 2007; Münder et al., 2010), but its role in embryonic tentacle development is unknown. Although more data are needed from *Hydra* embryonic development, these previous results provide further evidence that the tentacle development program might be very different between *Hydra* and *Nematostella*.

Epithelial placodes as a common theme in organ and appendage outgrowth

It is well established that thickened epithelial placodes (similar to those described here) play a role in the development of various tissues and organs of bilaterian organisms. The imaginal discs of *Drosophila*, for example, are larval primordia that give rise to all the appendages of the adult body (Cohen, 1993). These structures all develop as pseudostratified epithelial placodes prior to undergoing radical metamorphic cell shape changes that result in elongation of the larval epithelia into their adult forms (Fristrom, 1988). Placodes are also central to the development of outgrowths in vertebrate systems, including hair follicles, teeth, feathers, ears and the lens of the eye (Baker and Bronner-Fraser, 2001; Pispa and Thesleff, 2003; Streit, 2007). Remarkably, it remains poorly understood why thickened epithelial primordia are such a common theme in animal development. We have now shown that a similar mechanism occurs during appendage morphogenesis of a basal metazoan, indicating deep evolutionary constraints that favor this cellular mechanism regardless of its molecular basis in each lineage.

There are two potential scenarios for the evolution of placodal development. The first is that placodal development is a conserved feature inherited from the common cnidarian-bilaterian ancestor. In this situation, *Hydra* might represent a derived situation in which the placode-dependent mechanism for tentacle development has been lost. Investigation of additional cnidarian species, especially

anthozoans, would be needed to support this contention. The second possibility is that the appearance of epithelial placodes throughout Metazoa is a product of convergent evolution, appearing independently in multiple lineages. Currently, the sensory placodes of vertebrates are the best studied in the light of evolution, yet prior to recent data from chordates and urochordates these were thought to be a vertebrate innovation (Graham and Shimeld, 2013). The evolution of mechanisms to control the development of integumental placodes (which give rise to the ectodermal appendages of vertebrates) has not been addressed, although there do seem to be common molecular themes (Mikkola, 2007). Nevertheless, more invertebrate and basal metazoan species would need to be examined before there are sufficient data to support a definitive hypothesis.

Regardless of the evolutionary scenario, the widespread appearance of placodes in animal embryos indicates a crucial utility in the formation and patterning of secondary outgrowths of the main body axis. This raises the question of why placodal development is such an important mechanism. Using a thickened placode where the cells are packed closely together might allow for the high density patterning of a large primordial structure in a relatively small space. Once the pattern is formed, morphogenesis of the epithelium through changes in apicobasal cell thickness could then directly expand the primordium into a larger structure, organ or outgrowth.

Acknowledgements
We thank Karin Zueckert-Gaudenz, Brian Fleharty and Allison Peak for preparing and hybridiziding the microarray samples; the Stowers Aquatic Core Facility and Diana Baumann for *Nematostella* husbandry; Mark Martindale for the ubiquitin-GFP plasmid; and Lynnette Gutchewsky for administrative support.

Funding
This research was generously supported by the Stowers Institute for Medical Research and a Burroughs Wellcome Fund Career Award (to M.C.G.).

Competing interests statement
The authors declare no competing financial interests.

Supplementary material
Supplementary material available online at
http://dev.biologists.org/lookup/suppl/doi:10.1242/dev.088260/-/DC1

References

Angelini, D. R. and Kaufman, T. C. (2005). Functional analyses in the milkweed bug Oncopeltus fasciatus (Hemiptera) support a role for Wnt signaling in body segmentation but not appendage development. *Dev. Biol.* **283**, 409-423.
Artavanis-Tsakonas, S. and Muskavitch, M. A. (2010). Notch: the past, the present, and the future. *Curr. Top. Dev. Biol.* **92**, 1-29.
Baker, C. V. and Bronner-Fraser, M. (2001). Vertebrate cranial placodes I. Embryonic induction. *Dev. Biol.* **232**, 1-61.
Benjamini, Y. and Hochberg, Y. (1995). Controlling the false discovery rate: a practical and powerful approach to multiple testing. *J. R. Stat. Soc. B* **57**, 289-300.
Bode, H. R. (2001). Role of Hox genes in axial patterning in Hydra. *Am. Zool.* **41**, 621-628.
Bode, H. R. and David, C. N. (1978). Regulation of a multipotent stem cell, the interstitial cell of hydra. *Prog. Biophys. Mol. Biol.* **33**, 189-206.
Bouillon, J. (1994). Embranchement des cnidaires (Cnidaria). In *Traité de Zoologie. Cnidaires, Cténaires* (ed. P. P. Grassé). Paris: Masson.
Broun, M. and Bode, H. R. (2002). Characterization of the head organizer in hydra. *Development* **129**, 875-884.
Broun, M., Gee, L., Reinhardt, B. and Bode, H. R. (2005). Formation of the head organizer in hydra involves the canonical Wnt pathway. *Development* **132**, 2907-2916.
Campbell, R. D. (1967a). Tissue dynamics of steady state growth in Hydra littoralis. I. Patterns of cell division. *Dev. Biol.* **15**, 487-502.
Campbell, R. D. (1967b). Tissue dynamics of steady state growth in Hydra littoralis. II. Patterns of tissue movement. *J. Morphol.* **121**, 19-28.
Casella, J. F., Flanagan, M. D. and Lin, S. (1981). Cytochalasin D inhibits actin polymerization and induces depolymerization of actin filaments formed during platelet shape change. *Nature* **293**, 302-305.
Chourrout, D., Delsuc, F., Chourrout, P., Edvardsen, R. B., Rentzsch, F., Renfer, E., Jensen, M. F., Zhu, B., de Jong, P., Steele, R. E. et al. (2006). Minimal ProtoHox cluster inferred from bilaterian and cnidarian Hox complements. *Nature* **442**, 684-687.
Cohen, S. M. (1993). Imaginal disc development. In *The Development of Drosophila melanogaster*, Vol. 2 (ed. M. Bate and A. Martinez Arias). Cold Spring Harbor, NY: Cold Spring Harbor Laboratory Press.
Collins, A. G., Schuchert, P., Marques, A. C., Jankowski, T., Medina, M. and Schierwater, B. (2006). Medusozoan phylogeny and character evolution clarified by new large and small subunit rDNA data and an assessment of the utility of phylogenetic mixture models. *Syst. Biol.* **55**, 97-115.
da Silva, S. M. and Vincent, J. P. (2007). Oriented cell divisions in the extending germband of Drosophila. *Development* **134**, 3049-3054.
David, C. N. and Campbell, R. D. (1972). Cell cycle kinetics and development of Hydra attenuata. I. Epithelial cells. *J. Cell Sci.* **11**, 557-568.
David, C. N. and Challoner, D. (1974). Distribution of interstitial cells and differentiating nematocytes in nests in Hydra attenuata. *Integr. Comp. Biol.* **14**, 537-542.
David, C. N. and Gierer, A. (1974). Cell cycle kinetics and development of Hydra attenuata. III. Nerve and nematocyte differentiation. *J. Cell Sci.* **16**, 359-375.
David, C. N. and Murphy, S. (1977). Characterization of interstitial stem cells in hydra by cloning. *Dev. Biol.* **58**, 372-383.
Denker, E., Manuel, M., Leclère, L., Le Guyader, H. and Rabet, N. (2008). Ordered progression of nematogenesis from stem cells through differentiation stages in the tentacle bulb of Clytia hemisphaerica (Hydrozoa, Cnidaria). *Dev. Biol.* **315**, 99-113.
Dovey, H. F., John, V., Anderson, J. P., Chen, L. Z., de Saint Andrieu, P., Fang, L. Y., Freedman, S. B., Folmer, B., Goldbach, E., Holsztynska, E. J. et al. (2001). Functional gamma-secretase inhibitors reduce beta-amyloid peptide levels in brain. *J. Neurochem.* **76**, 173-181.
Dunn, C. W., Hejnol, A., Matus, D. Q., Pang, K., Browne, W. E., Smith, S. A., Seaver, E., Rouse, G. W., Obst, M., Edgecombe, G. D. et al. (2008). Broad phylogenomic sampling improves resolution of the animal tree of life. *Nature* **452**, 745-749.
Finnerty, J. R. and Martindale, M. Q. (1999). Ancient origins of axial patterning genes: Hox genes and ParaHox genes in the Cnidaria. *Evol. Dev.* **1**, 16-23.
Finnerty, J. R., Paulson, D., Burton, P., Pang, K. and Martindale, M. Q. (2003). Early evolution of a homeobox gene: the parahox gene Gsx in the Cnidaria and the Bilateria. *Evol. Dev.* **5**, 331-345.
Franch-Marro, X., Martín, N., Averof, M. and Casanova, J. (2006). Association of tracheal placodes with leg primordia in Drosophila and implications for the origin of insect tracheal systems. *Development* **133**, 785-790.
Fristrom, D. (1988). The cellular basis of epithelial morphogenesis. A review. *Tissue Cell* **20**, 645-690.
Fritzenwanker, J. H. and Technau, U. (2002). Induction of gametogenesis in the basal cnidarian Nematostella vectensis (Anthozoa). *Dev. Genes Evol.* **212**, 99-103.
Geling, A., Steiner, H., Willem, M., Bally-Cuif, L. and Haass, C. (2002). A gamma-secretase inhibitor blocks Notch signaling in vivo and causes a severe neurogenic phenotype in zebrafish. *EMBO Rep.* **3**, 688-694.
Genikhovich, G. and Technau, U. (2009a). Anti-acetylated tubulin antibody staining and phalloidin staining in the starlet sea anemone Nematostella vectensis. *CSH Protoc.* **9**, pdb.prot5283.
Genikhovich, G. and Technau, U. (2009b). In situ hybridization of starlet sea anemone (Nematostella vectensis) embryos, larvae, and polyps. *CSH Protoc.* **9**, pdb.prot5282.
Gerhart, J. (1999). 1998 Warkany lecture: signaling pathways in development. *Teratology* **60**, 226-239.
Graham, A. and Shimeld, S. M. (2013). The origin and evolution of the ectodermal placodes. *J. Anat.* **222**, 32-40.
Hand, C. and Unlinger, K. R. (1992). The culture, sexual and asexual reproduction, and growth of the sea anemone Nematostella vectensis. *Biol. Bull.* **182**, 169-176.
Hassel, M., Albert, K. and Hofheinz, S. (1993). Pattern formation in Hydra vulgaris is controlled by lithium-sensitive processes. *Dev. Biol.* **156**, 362-371.
Hejnol, A., Obst, M., Stamatakis, A., Ott, M., Rouse, G. W., Edgecombe, G. D., Martinez, P., Baguna, J., Bailly, X., Jondelius, U. et al. (2009). Assessing the root of bilaterian animals with scalable phylogenomic methods. *Proc. Biol. Sci.* **276**, 4261-4270.
Holstein, T. W., Hobmayer, E. and David, C. N. (1991). Pattern of epithelial cell cycling in hydra. *Dev. Biol.* **148**, 602-611.
Irvine, K. D. and Wieschaus, E. (1994). Cell intercalation during Drosophila germband extension and its regulation by pair-rule segmentation genes. *Development* **120**, 827-841.
Käsbauer, T., Towb, P., Alexandrova, O., David, C. N., Dall'armi, E., Staudigl, A., Stiening, B. and Böttger, A. (2007). The Notch signaling pathway in the cnidarian Hydra. *Dev. Biol.* **303**, 376-390.

Keller, R. E. (1978). Time-lapse cinemicrographic analysis of superficial cell behavior during and prior to gastrulation in Xenopus laevis. *J. Morphol.* **157**, 223-247.
Keller, R. E. (1980). The cellular basis of epiboly: an SEM study of deep-cell rearrangement during gastrulation in Xenopus laevis. *J. Embryol. Exp. Morphol.* **60**, 201-234.
Kraus, P. and Lufkin, T. (2006). Dlx homeobox gene control of mammalian limb and craniofacial development. *Am. J. Med. Genet. A* **140**, 1366-1374.
Kusserow, A., Pang, K., Sturm, C., Hrouda, M., Lentfer, J., Schmidt, H. A., Technau, U., von Haeseler, A., Hobmayer, B., Martindale, M. Q. et al. (2005). Unexpected complexity of the Wnt gene family in a sea anemone. *Nature* **433**, 156-160.
Magie, C. R., Pang, K. and Martindale, M. Q. (2005). Genomic inventory and expression of Sox and Fox genes in the cnidarian Nematostella vectensis. *Dev. Genes Evol.* **215**, 618-630.
Manni, L., Lane, N. J., Joly, J. S., Gasparini, F., Tiozzo, S., Caicci, F., Zaniolo, G. and Burighel, P. (2004). Neurogenic and non-neurogenic placodes in ascidians. *J. Exp. Zool.* **302B**, 483-504.
Marlow, H. Q., Srivastava, M., Matus, D. Q., Rokhsar, D. and Martindale, M. Q. (2009). Anatomy and development of the nervous system of Nematostella vectensis, an anthozoan cnidarian. *Dev. Neurobiol.* **69**, 235-254.
Marlow, H., Roettinger, E., Boekhout, M. and Martindale, M. Q. (2012). Functional roles of Notch signaling in the cnidarian Nematostella vectensis. *Dev. Biol.* **362**, 295-308.
Martindale, M. Q., Pang, K. and Finnerty, J. R. (2004). Investigating the origins of triploblasty: 'mesodermal' gene expression in a diploblastic animal, the sea anemone Nematostella vectensis (phylum, Cnidaria; class, Anthozoa). *Development* **131**, 2463-2474.
Matus, D. Q., Thomsen, G. H. and Martindale, M. Q. (2007). FGF signaling in gastrulation and neural development in Nematostella vectensis, an anthozoan cnidarian. *Dev. Genes Evol.* **217**, 137-148.
Matus, D. Q., Magie, C. R., Pang, K., Martindale, M. Q. and Thomsen, G. H. (2008). The Hedgehog gene family of the cnidarian, Nematostella vectensis, and implications for understanding metazoan Hedgehog pathway evolution. *Dev. Biol.* **313**, 501-518.
Mazza, M. E., Pang, K., Martindale, M. Q. and Finnerty, J. R. (2007). Genomic organization, gene structure, and developmental expression of three clustered otx genes in the sea anemone Nematostella vectensis. *J. Exp. Zool.* **308B**, 494-506.
Mazza, M. E., Pang, K., Reitzel, A. M., Martindale, M. Q. and Finnerty, J. R. (2010). A conserved cluster of three PRD-class homeobox genes (homeobrain, rx and orthopedia) in the Cnidaria and Protostomia. *Evodevo* **1**, 3.
Meyer, E. J., Ikmi, A. and Gibson, M. C. (2011). Interkinetic nuclear migration is a broadly conserved feature of cell division in pseudostratified epithelia. *Curr. Biol.* **21**, 485-491.
Mikkola, M. L. (2007). Genetic basis of skin appendage development. *Semin. Cell Dev. Biol.* **18**, 225-236.
Münder, S., Käsbauer, T., Prexl, A., Aufschnaiter, R., Zhang, X., Towb, P. and Böttger, A. (2010). Notch signalling defines critical boundary during budding in Hydra. *Dev. Biol.* **344**, 331-345.
Petcherski, A. G. and Kimble, J. (2000). Mastermind is a putative activator for Notch. *Curr. Biol.* **10**, R471-R473.
Pires-daSilva, A. and Sommer, R. J. (2003). The evolution of signalling pathways in animal development. *Nat. Rev. Genet.* **4**, 39-49.
Pispa, J. and Thesleff, I. (2003). Mechanisms of ectodermal organogenesis. *Dev. Biol.* **262**, 195-205.
Putnam, N. H., Srivastava, M., Hellsten, U., Dirks, B., Chapman, J., Salamov, A., Terry, A., Shapiro, H., Lindquist, E., Kapitonov, V. V. et al. (2007). Sea anemone genome reveals ancestral eumetazoan gene repertoire and genomic organization. *Science* **317**, 86-94.
Rentzsch, F., Anton, R., Saina, M., Hammerschmidt, M., Holstein, T. W. and Technau, U. (2006). Asymmetric expression of the BMP antagonists chordin and gremlin in the sea anemone Nematostella vectensis: implications for the evolution of axial patterning. *Dev. Biol.* **296**, 375-387.
Ryan, J. F., Burton, P. M., Mazza, M. E., Kwong, G. K., Mullikin, J. C. and Finnerty, J. R. (2006). The cnidarian-bilaterian ancestor possessed at least 56 homeoboxes: evidence from the starlet sea anemone, Nematostella vectensis. *Genome Biol.* **7**, R64.
Ryan, J. F., Mazza, M. E., Pang, K., Matus, D. Q., Baxevanis, A. D., Martindale, M. Q. and Finnerty, J. R. (2007). Pre-bilaterian origins of the Hox cluster and the Hox code: evidence from the sea anemone, Nematostella vectensis. *PLoS ONE* **2**, e153.
Smith, K. M., Gee, L., Blitz, I. L. and Bode, H. R. (1999). CnOtx, a member of the Otx gene family, has a role in cell movement in hydra. *Dev. Biol.* **212**, 392-404.
Smyth, G. K. (2004). Linear models and empirical Bayes methods for assessing differential expression in microarray experiments. *Stat. Appl. Genet. Mol. Biol.* **3**, Article 3.
Streit, A. (2007). The preplacodal region: an ectodermal domain with multipotential progenitors that contribute to sense organs and cranial sensory ganglia. *Int. J. Dev. Biol.* **51**, 447-461.
Sullivan, J. C., Ryan, J. F., Watson, J. A., Webb, J., Mullikin, J. C., Rokhsar, D. and Finnerty, J. R. (2006). StellaBase: the Nematostella vectensis genomics database. *Nucleic Acids Res.* **34**, D495-D499.
Sullivan, J. C., Reitzel, A. M. and Finnerty, J. R. (2008). Upgrades to StellaBase facilitate medical and genetic studies on the starlet sea anemone, Nematostella vectensis. *Nucleic Acids Res.* **36**, D607-D611.
Szczepanek, S., Cikala, M. and David, C. N. (2002). Poly-gamma-glutamate synthesis during formation of nematocyst capsules in Hydra. *J. Cell Sci.* **115**, 745-751.
Trevino, M., Stefanik, D. J., Rodriguez, R., Harmon, S. and Burton, P. M. (2011). Induction of canonical Wnt signaling by alsterpaullone is sufficient for oral tissue fate during regeneration and embryogenesis in Nematostella vectensis. *Dev. Dyn.* **240**, 2673-2679.
Wei, Y. and Mikawa, T. (2000). Formation of the avian primitive streak from spatially restricted blastoderm: evidence for polarized cell division in the elongating streak. *Development* **127**, 87-96.
Wu, L., Aster, J. C., Blacklow, S. C., Lake, R., Artavanis-Tsakonas, S. and Griffin, J. D. (2000). MAML1, a human homologue of Drosophila mastermind, is a transcriptional co-activator for NOTCH receptors. *Nat. Genet.* **26**, 484-489.

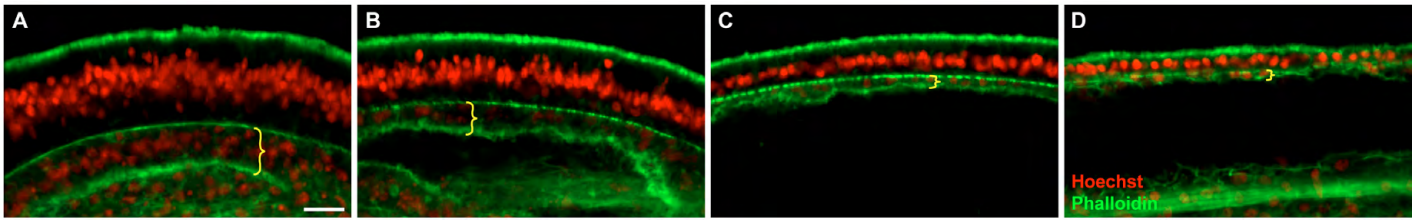

Fig. S1. Cell shape changes in the endoderm during development. (**A-D**) Animals at subsequent stages of development were stained with phalloidin to label F-Actin (green) and Hoechst to label nuclei (red). As the body column ectoderm progressively obtains a flattened morphology, the endoderm appears to make a similar transition. Brackets indicate the approximate thickness of the endodermal cell layer. Scale bar: 10 μm.

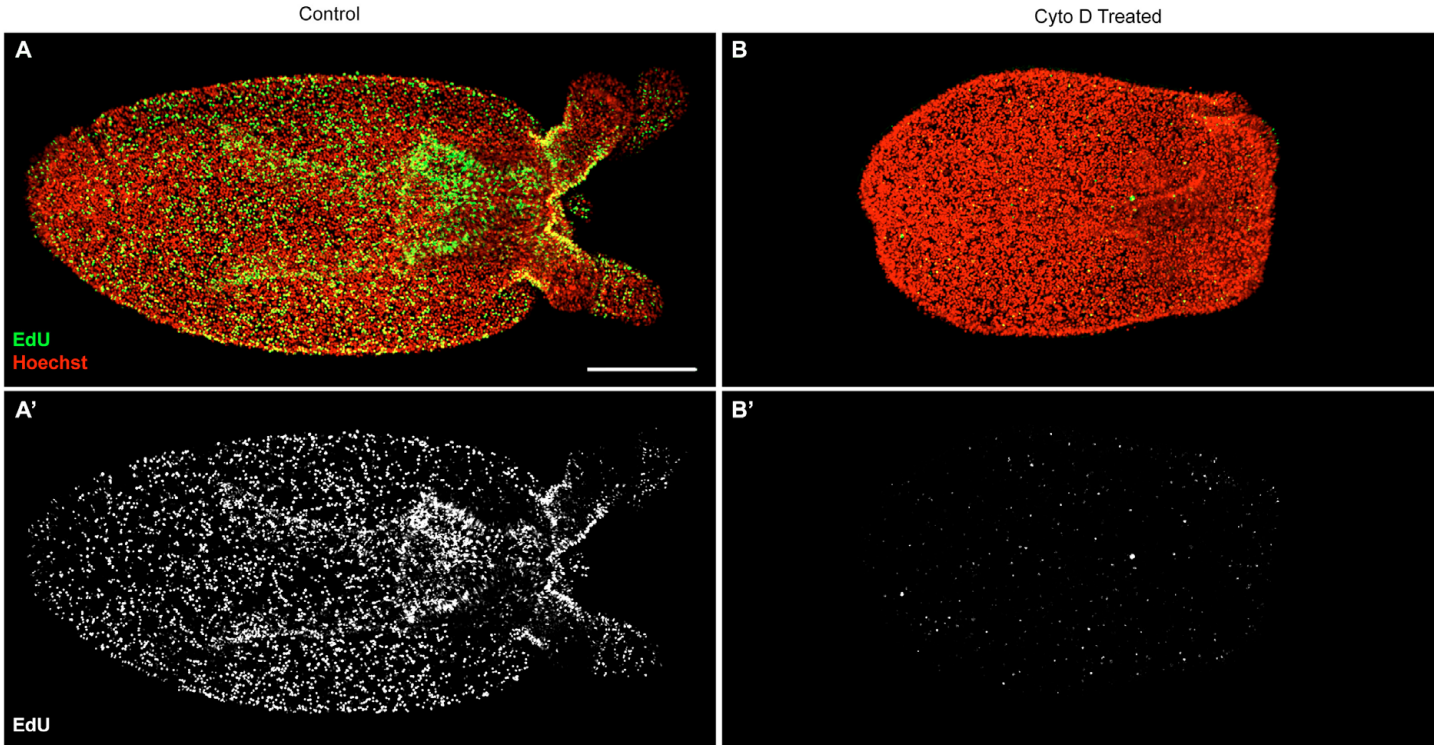

Fig. S2. Cell proliferation is reduced with Cyto D treatment. Control (**A**,**A′**) and Cyto D-treated (**B**,**B′**) animals were stained for EdU incorporation (green) and nuclei (Hoechst; red). Although Cyto D-treated animals still show some proliferation (B′), it is reduced compared with controls (A′). Scale bar: 100 μm.

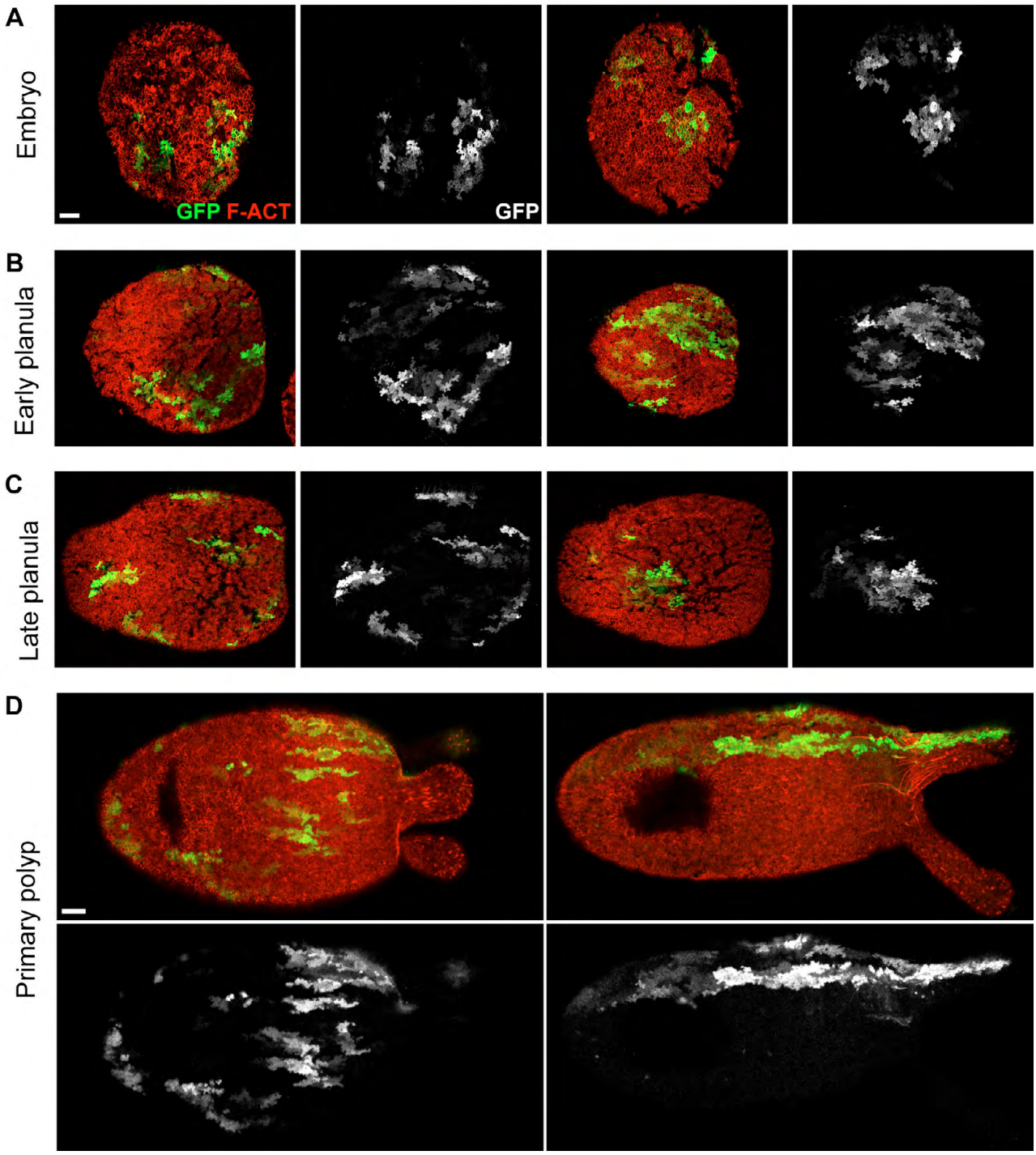

Fig. S3. Additional examples of Ubiquitin-GFP-injected animals showing the shape of ectodermal GFP-marked cell clusters during body column and tentacle elongation. GFP-marked cell clones (green) in animals stained with phalloidin to label F-Actin (red), showing additional examples of clone shape in embryos (**A**) and early planula larvae (**B**). Elongating cell clones appear in late planula larvae (**C**). Primary polyps exhibit highly elongated clones along the oral-aboral axis (**D**). Scale bars: 25 μm.

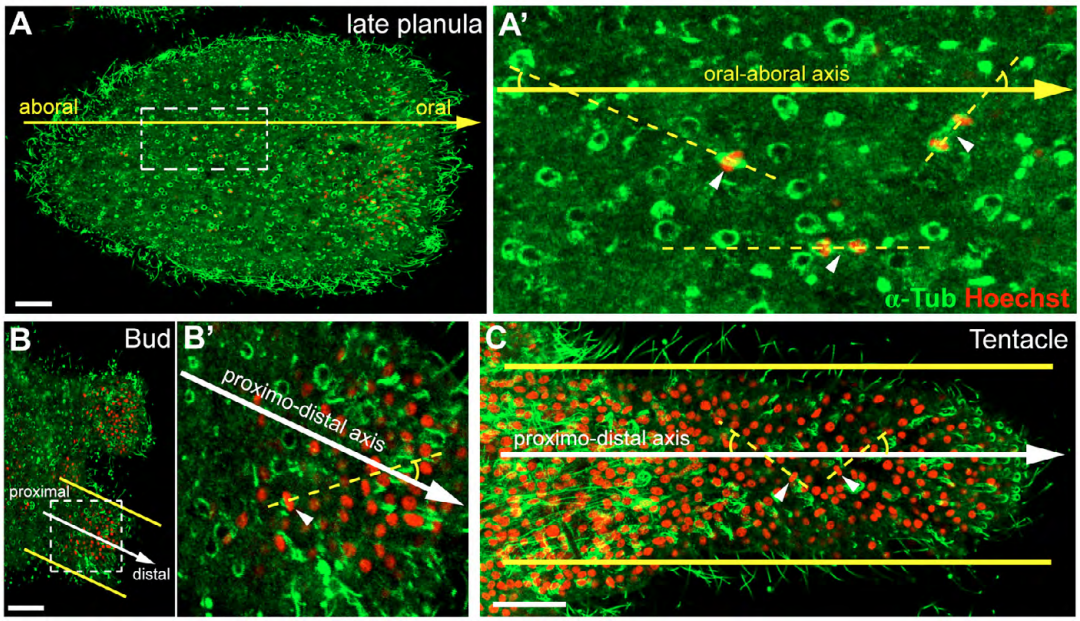

Fig. S4. Method for measurement of the orientation of cell division. (**A**,**A′**) During body column elongation, the angle between the mitotic spindle (dashed yellow line) and the oral-aboral axis (solid yellow arrow) was defined as the spindle angle. White arrowheads indicate mitotic figures. (**B-C**) In both developing buds (B,B′) and tentacles (C), the angle of the spindle was measured from the proximodistal axis (solid white arrow). This axis is parallel to the thickness of the bud and tentacle (solid yellow lines). Scale bars: 25 μm.

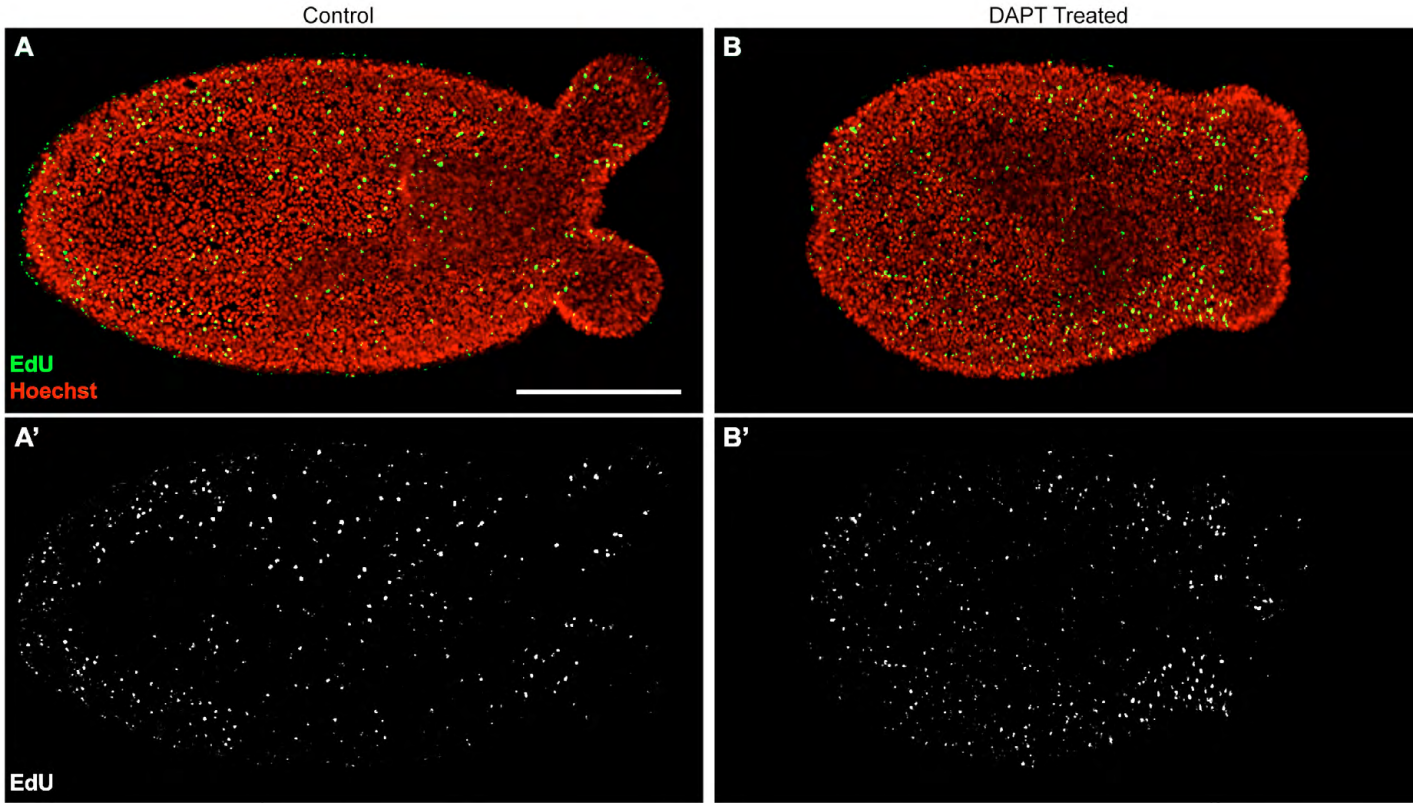

Fig. S5. Cell proliferation is not affected by inhibition of Notch signaling. (**A**,**B**) Confocal stacks of animals stained for EdU incorporation (green) and nuclei (Hoechst; red) for control (A) and DAPT-treated (B) animals. (**A′**,**B′**) EdU channel from A,B. DAPT-treated animals still had many EdU-positive cells (B′). Scale bar: 100 μm.

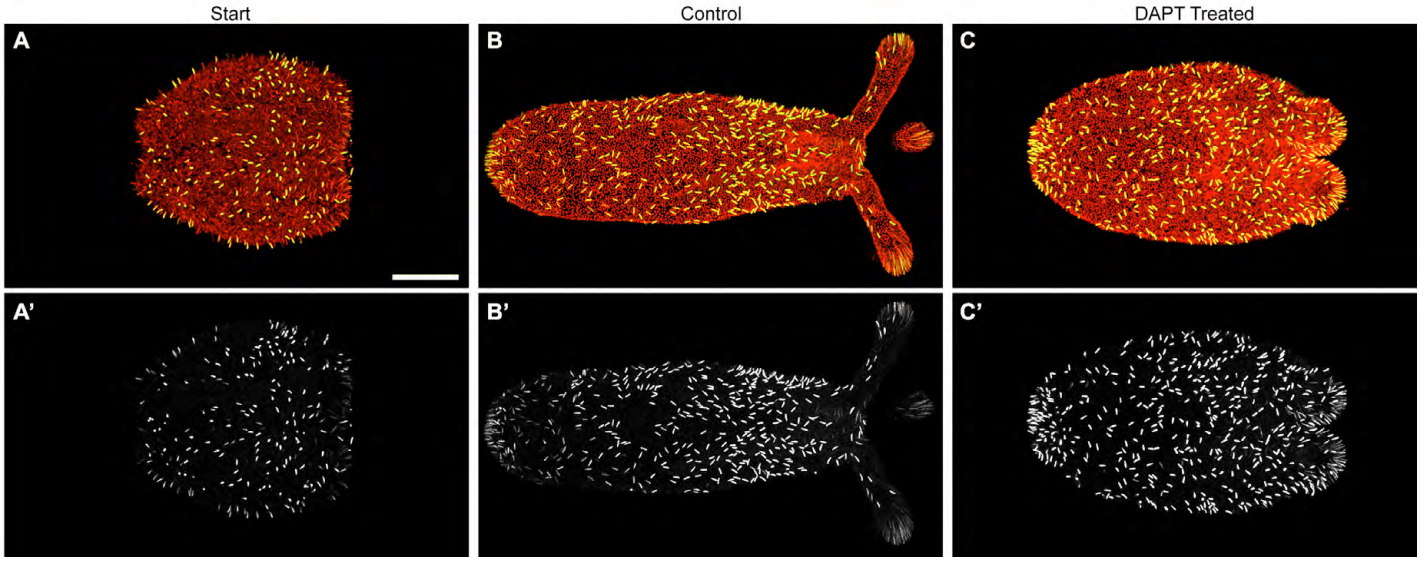

Fig. S6. Inhibition of Notch signaling during elongation did not dramatically alter cnidocyte localization. Confocal stacks of animals stained with DAPI to visualize cnidocytes. Animals at the start of the experiment (**A**,**A′**) had cnidocytes. Both control (**B**,**B′**) and DAPT-treated (**C**,**C′**) animals had many cnidocytes all over their bodies. Red channel shows nuclei and cnidocytes excited by the UV laser. The green channel and bottom row (A′-C′) show cnidocytes excited by the 488 laser. Scale bar: 100 μm.

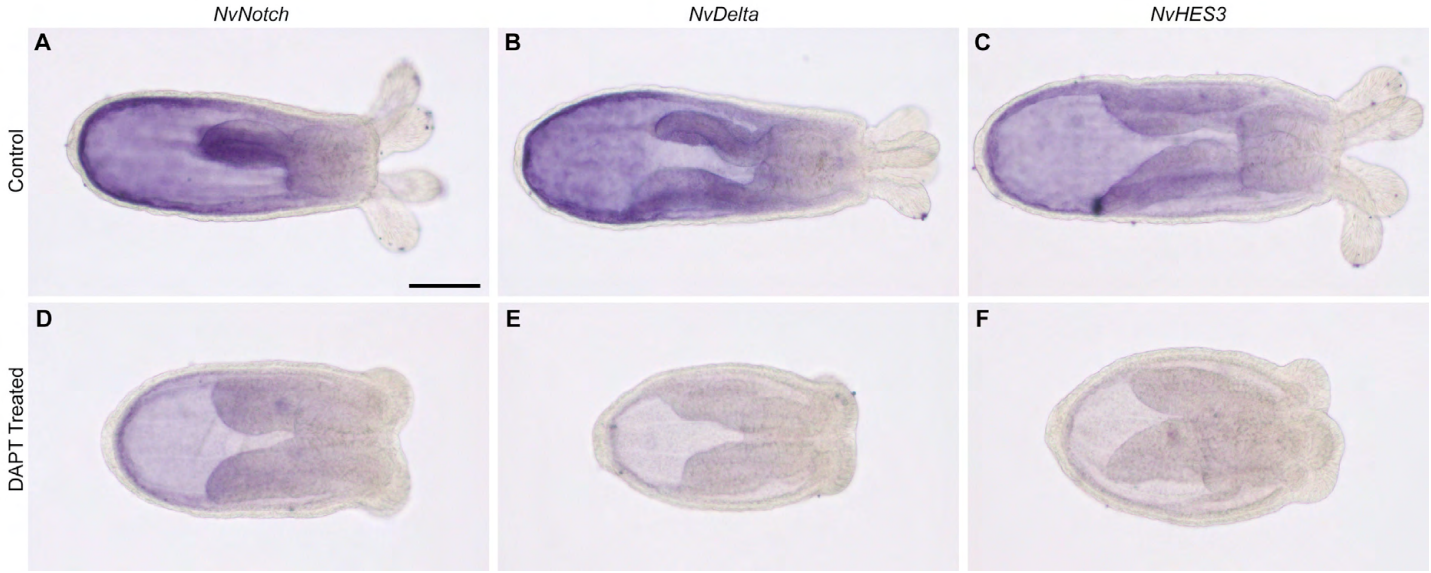

Fig. S7. Notch pathway components have unchanged expression patterns after DAPT treatment. (**A-C**) RNA *in situ* expression patterns of *NvNotch* (A), *NvDelta* (B) and *NvHES3* (C) in control animals. Expression of these transcripts was endodermal. (**D-F**) Corresponding expression patterns in DAPT-treated animals. All of the Notch pathway components had similar expression patterns in control and DAPT-treated animals. The DAPT-treated animals may downregulate all of these genes, as observed by reduced *in situ* staining. Scale bar: 100 μm.

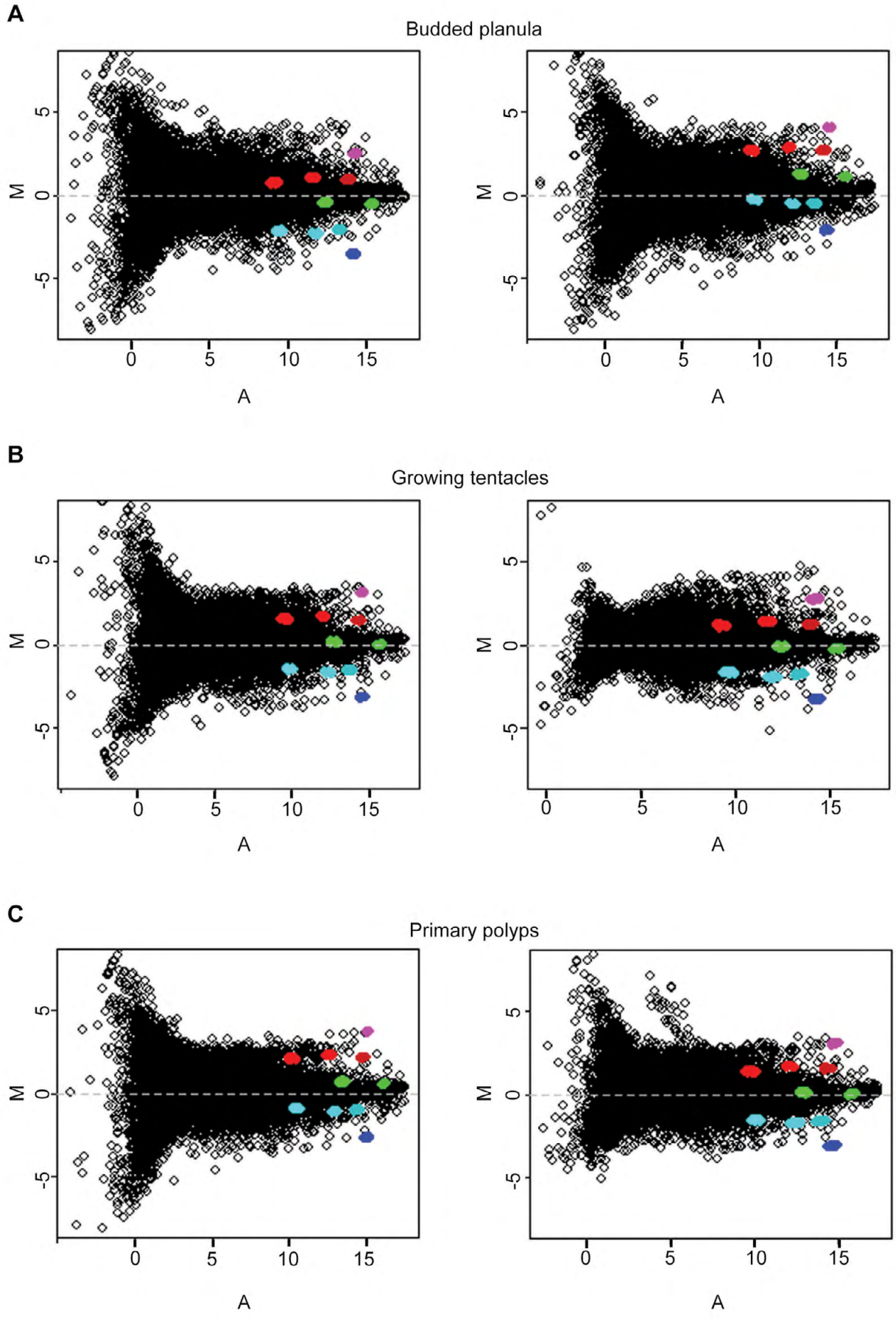

Fig. S8. Duplicate microarray analyses show high correlation and reproducibility. MA plots of normalized duplicate microarray analyses from budded planula (**A**), animals with growing tentacles (**B**) and primary polyps (**C**). Colored dots represent spots on the microarray. Duplicate experiments demonstrated consistent results.

Table S1. Genes screened by *in situ* hybridization after DAPT treatment

Sequence	Accession	Expression pattern change?
ZicC	AB231868	No
OtxA	FJ824849	No
OtxB	FJ824850	Yes
OtxC	FJ824851	No
Crossveinless-2	XM_001625111	No
Homeobrain	HM004558	No
Anthox2	AF085283.1	No
FoxL2	JGI: 82873608	No
Forkhead1	XM_001630267.1	No
Forkhead2	XM_001638841.1	No
Growth factor receptor	XM_001637818	No
G protein receptor	XM_001636348.1	No

Table S2. Tentacle domain markers identified in the microarray screen

Sequence	Accession	Primer pair for *in situ* probe
Anthox2	AF085283.1	CATGTCTTCGTCCTTCTACATTGACT AGGTTGCCCCGAATATAGTACATT
FoxL2	JGI: 82873608	ATTAACTGTGTCACACACAAGCGC TTCATGTACGGGTATACAGGAGGTAC
Forkhead1	XM_001630267.1	CACCGCACCACTGCAGCAAT CCTGCGACGGAAATTCCCCT
Forkhead2	XM_001638841.1	GGATGATGCAAAGCAAGCGA TCTCAGAGGGATGTTTAGCCGA
Growth factor receptor-like	XM_001637818	CTTGCACTCATTGACCGACATG ACGATTGGATTGCGTGGTTG
G protein receptor-like	XM_001636348.1	ATGTCCACAAACACAAGCACCTC AGAAAATCTTGTCGGCGGTCT

Table S3. *In situ* hybridization primer pairs

Sequence	Accession	Primer pair for *in situ* probe
OtxB	FJ824850	AAGAGCTGGGGGCCACGGATTACATC TATCTCGGCGCCATGGAATGCACG
Notch	JN982705	GCATGGGCTTTGCTTGGATT CAGTTACTCCCAGTGTATCCAGGTCT
Delta	JN982706	ATGCAGCTACTACCACTCCAGCCA GACACGCGCCATCAAAGCAA
HES3	JN982709	GGCCGTTGACTGCATCGATA TGTGCTGACGATAGTCGTCTGC